sediment transport in rivers

flow of water in a curved open channel with a fixed uneven bed

H. J. de Vriend and F.G. Koch

report on experimental and theoretical investigations

R 657-VI
M 1415 part II

November 1978

toegepast onderzoek waterstaat

CONTENTS

LIST OF TABLES

LIST OF FIGURES

LIST OF SYMBOLS

a_1, a_2	Constants in the elaboration of the measured data, theoretically equal to h/R and tanα respectively
B	Channel width
c_1	Slope of the calibration curve of the velocity meter
c_2	Value of the velocity corresponding to zero pulse frequency
c_{2_0}	Value of c_2 at calibration temperature
c_3	Coefficient of proportionality in the direction measurement
c_4	Coefficient of proportionality in the temperature correction of c_2
C	Local value of Chézy's roughness factor
C_o	Value of C at the reference depth of flow h_o
$\underline{d}$	Depth of flow scale in the numerical simulation of the flow
e	Energy head
$\bar{e}$	Mean value of e in the relevant cross-section
$f_{main}(\frac{z}{h})$	Vertical distribution function of the main velocity component
$f_{sec}(\frac{z}{h})$	Vertical distribution function of the helical velocity component
$f_\phi(\frac{z}{h})$	Vertical distribution function of the flow deviation angle (ϕ-α)
	Froude number based on the overall mean velocity and $\underline{d}$
g	Acceleration due to gravity
h	Local depth of flow
h_o	Reference depth of flow for Chézy's factor
i	Number of the grid point (i = 1 near the bed)
I_s	Longitudinal slope of the energy line
k	Nikuradse roughness length (equivalent sand roughness)
N	Number of pulses counted by the velocity meter during an observation
np	Number of grid points in a vertical
Q	Discharge
R	Local radial coordinate
R_s	Radius of curvature of the streamlines of the depth-averaged flow field
s	Time-mean reading of the potentiometer during flow direction measurements
s_o	Reference reading of the potentiometer during flow direction measurements
T	Duration of the observation period for a velocity measurement
$\tilde{v}$	Estimate of the mean velocity when determining C from the measured velocities in the lower parts of a vertical
v_{hel}	Local time-mean helical velocity component

LIST OF SYMBOLS (continued)

$\tilde{v}_{hel}$	Secondary flow intensity
v'_{hel}	Normalized helical velocity component
v_{main}	Local time-mean main velocity component
$\bar{v}_{main}$	Depth-averaged value of v_{main}
$\tilde{v}_{main}$	Estimate of the depth-averaged velocity in the elaboration of the measured data
v'_{main}	Normalized main velocity
v_r	Local time-mean radial velocity component
$\bar{v}_r$	Depth-averaged value of v_r
v_t	Local time-mean tangential velocity component
$\bar{v}_t$	Depth-averaged value of v_t
v_{tot}	Local time-mean total velocity
$\bar{v}_{tot}$	Depth-averaged value of v_{tot}
V_{main_i}	Main velocity in grid point i, calculated from measured data
y	Transverse coordinate (y = 0 at the left bank)
z	Vertical distance to the bed
z_s	Water surface elevation
$\bar{z}_s$	Mean value of z_s in the relevant cross-section
z_o^*	Level at which the logarithmic velocity distribution becomes equal to zero
α	Direction of the depth-averaged velocity vector
η_m	Dynamic viscosity of water at the measuring temperature
η_c	Dynamic viscosity of water at the calibration temperature
κ	Von Kármán's constant
ϕ	Local time-mean flow angle with respect to the channel axis
ϕ'	Local time-mean flow angle, read from the flow direction meter
ϕ'_o	Reference flow angle, read from the flow direction meter

SUMMARY

This report describes physical and numerical experiments on the steady flow of water in a curved flume, consisting of a 38 m long straight section followed by a 90^{o} bend with a radius of curvature of 50 m (see Figure 1). The cross-section was formed by two vertical side walls and a concrete bed with a schematized large-scale bed configuration as can be expected in a natural river bend. The width of the flume was 6 m and the depth of flow varied between 0.05 m and 0.4 m, with a mean value of about 0.2 m. Measurements were taken at two discharges: 0.463 m^3/s and 0.232 m^3/s (yielding mean velocities of about 0.4 m/s and 0.2 m/s respectively).

During the experiments the following phenomena were investigated:

a. the vertical distribution of the horizontal velocity components v_{main} (in the main flow direction) and v_{hel} (perpendicular to the main flow direction);
b. the horizontal distribution of the depth-averaged velocity and the intensity of the secondary flow; and
c. the water surface configuration and the distribution of the energy head.

The experimental results have been compared with the results of a mathematical model of steady flow in curved open channels, developed in the Laboratory of Fluid Mechanics of the Delft University of Technology (de Vriend, 1976 and 1977).

The vertical distributions of the main velocity turned out to be highly similar throughout the flow field, but they all were somewhat flatter than predicted by the logarithmic profile used in the mathematical model.
The vertical distributions of the helical velocity (i.e. the shape of the curve) agreed well with the theoretical curve in the deeper parts of the bend, but in the shallower parts the measured data were too inaccurate to draw conclusions.
The observed depth-averaged velocity field showed an important deviation from the predicted one: the observed shifting of the velocity maximum towards the outer wall in the bend was considerably stronger. This phenomena, which was also encountered during earlier experiments with a plane bed (de Vriend and Koch, 1977), must be attributed to the advective influence of the secondary flow, which is not incorporated in the mathematical model.
The observed intensity of the secondary flow was considerably stronger than the predicted one, which is in accordance with the results of the plane bed experiments.
The computed configurations of the water surface and the energy surface deviated

from the measured data in that respect that the longitudinal head losses were larger, and a different transverse slope of the water surface in the bend was found. An important part of these differences can be explained from the differences between the computed and the measured depth-averaged velocity fields.

FLOW OF WATER IN A CURVED OPEN CHANNEL WITH A FIXED UNEVEN BED

1 Introduction

This report is a continuation of the report R 657-V/M 1415, Part I, "Flow of water in a curved channel with a fixed plane bed" (de Vriend and Koch, 1977). The investigations described in both reports were executed within the applied research group for sediment transport in rivers, in which Rijkswaterstaat Directorate for Water Management and Research, the Delft Hydraulics Laboratory, and the Delft University of Technology collaborate. This project is incorporated in the basic research program TOW (Toegepast Onderzoek Waterstaat: Applied Research Waterstaat). Further information on the background of the experiments is given in Part I.

Part I describes experiments in a wide shallow curved channel with a fixed plane bed and a rectangular cross-section. The present report gives the results of a series of experiments executed in the same flume with a fixed uneven bed having a large-scale configuration as in a natural river bend. For this type of experiment little data have been reported in literature (de Vriend, 1976; Yen, 1967 and 1970).
The results of the experiments have been compared with the results of a mathematical model of steady flow in curved open channels, developed at the Laboratory of Fluid Mechanics of the Delft University of Technology (de Vriend, 1976). Such a comparison is thought to be even more important for testing the mathematical model than a comparison with the results of the earlier flat bed experiments, as the channel configuration was close to the natural one.

The experiments have been executed by Mr. H.J. de Vriend of the Delft University of Technology and by Mr. F.G. Koch of the Delft Hydraulics Laboratory.

2 Experimental set-up

2.1 Channel geometry

During the experiments, described in this report, the flow (velocity and direction) and the elevation of the free water surface were measured in a curved flume with a fixed uneven bed having a large-scale configuration as in a natural river bend.

The geometry of the channel is shown in Figures 1 and 2. The plan-view consisted of a 38 m long straight section, followed by a 90^{o} bend with a radius of curvature of 50 m (see Figure 1). The channel width was 6 m and the bed elevation varied as shown in Figure 2a. In the straight section (cross-sections A_0, A_1, A_2, B_0) the channel was prismatic, with a parabolic shape of the bed and a zero longitudinal slope (see Figure 2b). Between cross-sections B_0 and C_0 the bed elevation gradually changed from a parabolic cross-section to a cross-section with a point bar near the inner wall and a deeper channel near the outer wall (see cross-section C_0 in Figure 2a). All subsequent cross-sections (C_1, D_0, D_1 and E_0) had the same configuration as C_0, but were sloping downward with a slope of $3 * 10^{-4}$ along the channel axis (see Figure 2b).

2.2 Flow conditions

Two series of measurements were carried out, one with a discharge of 0.463 m^3/s, and the other with a discharge of 0.232 m^3/s. During both series the water surface elevation at the upstream boundary of the channel was kept constant, so that the depth of flow in the channel axis was about 0.26 m, (yielding average velocities of about 0.4 m/s and 0.2 m/s respectively). The discharge and the water surface elevation were regulated with a movable Romijn-weir and a tail-gate as described in Part I.

The water inflow at the upstream end of the channel was adjusted in such a way that the distribution of the depth-averaged velocity in section A_1 agreed with a theoretical distribution. The latter was derived by applying Chézy's law to all streamlines, supposing the channel to be straight and prismatic, with a longitudinal slope of the energy line that is constant in a cross-section. Figure 3 shows that for $Q = 0.463$ m^3/s the mean velocity, estimated by the velocity measured at 0.4 h above the bed, was in good agreement with this theoretical distribution.

At the downstream end of the flume the water level was regulated by a tail gate. When the edge of this tail gate was kept horizontal, the flow was drawn towards the inner wall due to the uneven drawdown caused by the bed configuration. Therefore the edge was made oblique, with the highest point near the inner side wall, so that the flow pattern in section E_0, and particularly the mean flow angle α, was about the same as in section D_1.

2.3 Measured data

The experimental testing of the mathematical model was concentrated on the following phenomena:

- The vertical distributions of the horizontal velocity components (main flow and helical flow) (T7 and 8, for a summary of the tests see Table I);
- the horizontal distributions of the total depth-averaged velocity and the secondary flow intensity (T8); and
- the horizontal distribution of the water surface elevation and the energy head (T9).

In order to gather experimental information about these phenomena, the time-averaged magnitude and direction of the velocity vector were measured in a three-dimensional grid, using a combined current-velocity/direction meter, and the water surface elevation was measured in selected verticals of this grid, using static tubes (see Appendix A).
The measuring procedure used is described and motivated in Appendix B.

The grid points were defined by 9 cross-sections (numbered A_1 to E_0; see Figure 1a), 13 equidistant verticals in each cross-section (numbered 1 to 13, see Figure 1b), and a number of grid points per vertical varying from 2 to 10 according to the depth of flow in the relevant vertical. The minimum distance between two grid points in a vertical was 0.01 m.

Cross-section A_0, situated close to the upstream boundary, turned out to be unsuitable for inclusion in the grid as the flow was not yet fully developed there.

3 Results

3.1 Elaboration of the measured data

The elaboration procedure described in Appendix C was used to split up the measured velocities into a main and a helical component, parallel and perpendicular to the streamlines of the depth-averaged flow field respectively. The main outlines of this procedure agree with those of the procedure used for the rectangular channel data (de Vriend and Koch, 1977), but an attempt was made to prevent one of the main sources of errors, viz., the trapezoidal integration rule (de Vriend, 1978), by replacing the averaging in the vertical by a fitting of the measured data to given theoretical curves. The normalized main and helical velocity components and the depth-averaged flow field resulting from this elaboration are dealt with later in this Chapter.
As the elaboration procedure, however, can only be used if Chézy's constant C is given, some attention must be paid to this constant first. Because it must be expected to depend on the local depth of flow h, a relation between C and h must be given. The roughness of the channel shows no large variations, so the equivalent roughness length of the bed can be assumed to be constant everywhere in the channel. In addition, the bed may be expected to be hydraulically rough (Nikuradse roughness length $k \approx 1 * 10^{-3}$ m; viscous sublayer thickness $\approx 5 * 10^{-4}$ m), so that the following logarithmic relation between C and the local depth of flow h can be derived from the White-Colebrook formula for shallow channels:

$$C = C_o + 18\ {}^{10}\log(h/h_o)\ , \qquad (1)$$

in which C_o denotes the value of C at the reference depth of flow h_o. There are various possibilities to estimate C_o, such as:

- The White-Colebrook formula for a hydraulically rough bed:

$$C_o = 18\ {}^{10}\log \frac{12h_o}{k}\ , \qquad (2)$$

  where k denotes the equivalent sand roughness according to Nikuradse. For $k = 1 * 10^{-3}$ m and $h_o = 0.25$ m, this yields $C_o = 62\ m^{\frac{1}{2}}/s$.
- Chézy's law applied to the straight section upstream. In combination with (1) this yields:

$$C_o = \frac{Q}{B\, h_o^{3/2}\, I_s^{1/2}} \; \frac{1}{\int_0^1 \left(\frac{h}{h_o}\right)^{3/2} d\left(\frac{y}{B}\right)} - 18 \frac{\int_0^1 \left(\frac{h}{h_o}\right)^{3/2} {}^{10}\log\left(\frac{h}{h_o}\right)\, d\left(\frac{y}{B}\right)}{\int_0^1 \left(\frac{h}{h_o}\right)^{3/2} d\left(\frac{y}{B}\right)}, \qquad (3)$$

in which Q is the total discharge, B is the channel width, I_s is the slope of the energy line and y is a horizontal coordinate perpendicular to the channel axis (y = 0 at the left bank, y = B at the right bank). For the present experiments the values of C_o found in this way were 58 $m^{\frac{1}{2}}/s$ for Q = 0.463 m^3/s and 61 $m^{\frac{1}{2}}/s$ for Q = 0.232 m^3/s.

- Graphical representation of the measured main velocity distributions in semi-logarithmic plots, estimating the main velocity by the total velocity (if the secondary flow is relatively weak) or by the main velocity obtained from an elaboration based on the trapezoidal integration. A logarithmic velocity distribution plotted this way yields a straight line under a slope of

$$\frac{d(v_{main})}{d({}^{10}\log \frac{z}{h})} = \frac{\sqrt{g}}{\kappa C} \frac{\bar{v}_{main}}{0.435}, \qquad (4)$$

where $\bar{v}_{main}$ is the mean velocity in the relevant vertical. So C (and hence, through (1), C_o) can be estimated from the slope of a straight line fitted through the plotted data. This method was applied to the rectangular channel data to yield C = 70 $m^{\frac{1}{2}}/s$ at the higher and C = 50 $m^{\frac{1}{2}}/s$ at the lower discharge (de Vriend and Koch, 1977).

- Fitting the logarithmic curve

$$v_{main} = \tilde{v}\ (1 + \frac{\sqrt{g}}{\kappa C} + \frac{\sqrt{g}}{\kappa C} \ln \frac{z}{h}) \qquad (5)$$

through the main velocities measured in the lower points of a vertical, starting from the assumption that the velocity distribution is logarithmic near the bed.*) Adopting a least-squares method to determine the constants $\tilde{v}$ and $\frac{\sqrt{g}}{\kappa C}$ in each vertical, C_o can be derived form C through (1). In the present experiments this yielded values of C_o in the straight channel section of about 70 $m^{\frac{1}{2}}/s$.

---

* This method differs from the foregoing one in that the logarithmic distribution is assumed close to the bed rather than in the whole vertical. Consequently, the unknown constant $\tilde{v}$ figures in (5) instead of the vertical mean velocity $\bar{v}_{main}$.

Without discussing the accuracy of the various methods, C_o has been chosen 60 $m^{\frac{1}{2}}/s$ for both discharges and h_o = 0.25 m.

3.2 Vertical distribution of the main velocity component

In order to make the vertical distributions of the main velocity comparable from vertical to vertical, v_{main} has been normalized by its vertical mean value $\bar{v}_{main} = \bar{v}_{tot}$ (see Appendix C):

$$v'_{main} = \frac{v_{main}}{\bar{v}_{tot}} . \qquad (6)$$

In accordance with the rectangular channel case, this normalized main velocity distribution has been more closely examined with relation to two questions that are important in the development of a mathematical model of curved channel flow (de Vriend, 1976 and 1977):

- to what extent is v'_{main} similar from vertical to vertical? and
- can the distribution be described by the logarithmic profile? So

$$v'_{main} = 1 + \frac{\sqrt{g}}{\kappa C} + \frac{\sqrt{g}}{\kappa C} \ln \left(\frac{z}{h}\right) . \qquad (7)$$

Compared with the rectangular channel case, however, complications arise here from the variation of the depth of flow, leading to variations in C (for the present variation of h, C varies between 40 and 65 $m^{\frac{1}{2}}/s$, if C_o = 60 $m^{\frac{1}{2}}/s$ and h_o = 0.25 m). As v'_{main} is most likely to depend on C, this implies that, as long as the relationship between v'_{main} and C has not been established (cf. (7)), only verticals with approximately the same values of C, i.e., the same depth of flow, can be considered when investigating similarity. Therefore the verticals have been grouped according to their depth of flow in Table II, and a selection of verticals from each group was used to investigate similarity.

In Figure 4, representing the main velocity distributions in three classes of C (and h) for the two discharges, no significant differences between the various verticals in a class can be observed, except may be for C = 60 - 65 $m^{\frac{1}{2}}/s$, where the main velocity near the bed tends to be higher in the bend than in the straight section (Figures 4c and 4f).
Figure 5 shows the distributions of the quantity $\frac{\kappa C}{\sqrt{g}} (v'_{main} - 1)$ in various verticals of each of the cross-sections A_1, C_0 and D_0. According to this figure, there is no or hardly any significant difference between the verticals of one cross-section.

When comparing the main velocity profiles with the logarithmic distribution (7), significant differences seem to occur (see Figures 4 and 5): in the lower part of a vertical the measured velocities are higher than predicted by (7), and in the upper part, especially close to the water surface, they are lower. Although these differences occur throughout the flow and at both discharges, they tend to be the largest in the bend and at the higher discharge (see Figure 5). According to Figure 4, the dependency of the above-mentioned differences on the place in the flume (bend or straight section) hardly violates similarity. Hence it is concluded that a similarity approximation can be made for the main velocity. Regarding the applicability of the logarithmic curve, the differences between the measured data and (7) give rise to reservations not only for the present case of an uneven bed, but also for a plane bed, where these differences are qualitatively and quantitatively the same (Figure 6; see also de Vriend and Koch, 1977).

3.3 Vertical distribution of the helical velocity component

The helical velocities in the various verticals of a class of C and h are made comparable by normalizing v_{hel} by

$$v'_{hel} = \frac{v_{hel}}{\tilde{v}_{hel}} , \tag{8}$$

in which $\tilde{v}_{hel}$ is determined for each vertical by fitting the theoretical curve

$$v'_{hel} = \frac{1}{\kappa^2} \{2 \int_{z_o^*/h}^{z/h} \frac{\ln (\frac{z}{h})}{\frac{z}{h} - 1} d(\frac{z}{h}) + \frac{\sqrt{g}}{\kappa C} \int_{z_o^*/h}^{z/h} \frac{\ln^2 (\frac{z}{h})}{\frac{z}{h} - 1} d(\frac{z}{h}) -$$

$$- 2(1 - \frac{\sqrt{g}}{\kappa C}) v'_{main}\} \tag{9}$$

with $\frac{z_o^*}{h} = \exp(- 1 - \frac{\kappa C}{\sqrt{g}})$ and v'_{main} as given in (7), to the measured helical velocities (see Appendix C).

Figure 7 shows the helical velocities normalized in this way for three classes of C and for the two discharges. Except for C = 50 - 55 $m^{\frac{1}{2}}/s$, where the measured data are widely scattered due to the small number of measuring points in a vertical and the small values of the helical velocity component, the measured data lie within a narrow band and no significant differences occur between the various verticals in a class.

In addition, the data lie close to the theoretical curves representing (9), except for C = 60 - 65 $m^{\frac{1}{2}}/s$, where $|v'_{hel}|$ tends to be larger near the bed and smaller near the surface. These deviations are in qualitative agreement with the deviations of the normalized main velocity from the logarithmic curve (see Figure 5), the "source" of the secondary circulation being $\frac{\partial}{\partial z}\left(\frac{v^2_{main}}{R_s}\right)$ if R_s denotes the radius of curvature of the streamlines of the depth-averaged flow field (Rozovskii, 1961; de Vriend, 1973 and 1978).
The conclusions drawn from these results are:

- The helical velocity component permits a similarity approximation, and
- the theoretical curve (9) gives a good description of the vertical distribution of v_{hel} if the vertical distribution of the main velocity deviates only slightly from the logarithmic profile.

3.4 Depth-averaged velocity field

Appendix C describes the elaboration of the measured data, yielding i.e. the depth-averaged velocity $\bar{v}_{tot}$. The resulting distributions are given in Table III and Figure 8.
The depth-averaged velocity field has also been simulated numerically using a computer programme developed at the Laboratory of Fluid Mechanics of the Delft Hydraulics University of Technology (de Vriend, 1976 and 1977). The computational grid consisted of a cartesian part, covering the straight part of the flume from section A_0 on, and a polar part, covering the curved part of the flume up to section E_0. The longitudinal step size was 1.00 m in the channel axis, while the transverse step size was 6.00/16 = 0.375 m. At the upstream boundary the measured mean velocity distribution and the corresponding vorticity distribution were imposed. At the downstream boundary a linear profile was adopted for the surface elevation, so that the mean transverse slope was the same as the measured one. In addition, the following values of the constants were introduced: $\kappa = 0.4$; and C = 60 $m^{\frac{1}{2}}/s$ for $\underline{d}$ = 0.2 m and Fr = 0.275 and 0.138 for the higher and the lower discharge respectively. The main velocity distributions resulting form the numerical simulation of the flow are given in Figure 8. Comparison with the measured data shows the mathematical model to fail at essentially the same point as in case of a plane bed (cf. de Vriend and Koch, 1977): the shifting of the velocity maximum towards the outer wall is inadequately predicted. As in the plane bed case, this shortcoming must be attributed to the advective influence of the secondary flow on the main flow, which is not included in the mathematical model.

This is readily illustrated by the good agreement between the measured and the predicted distributions of $\bar{v}_{tot}$ in the shallow part of the cross-sections D_0 through E_0, where the intensity of the secondary flow, and hence its advective influence, is small.
From these results it must be concluded that, in spite of the great influence of the bed configuration on the mean velocity distribution, the discrepancy between the measured and the predicted velocity fields is considerable. This is in contrast with what had earlier been expected (de Vriend and Koch, 1977) on the basis of conclusions drawn from simulations of uneven bed flow (Engelund, 1974; de Vriend, 1976 and 1977).

3.5 Intensity of the secondary flow

One of the quantities resulting from the elaboration of the measured data in a vertical is $\tilde{v}_{hel}$, which can be considered as a measure of the secondary flow intensity in the relevant vertical. According to Figure 9, showing the distribution of $\tilde{v}_{hel}$ in the various cross-sections, the secondary flow intensity is considerable only in the deeper parts of the bend, with the highest values in section C_0. There the curvature of the contour lines of the bed is the largest and consequently the curvature $1/R_s$ of the streamlines of the depth-averaged flow field (and hence the source of the secondary flow) is likely to reach its maximum near this cross-section.
According to the theory underlying the numerical model (de Vriend, 1976 and 1977; also Rozovskii, 1961), $\tilde{v}_{hel}$ is equal to $\bar{v}_{tot} h/R_s$. Therefore $\tilde{v}_{hel}$ is compared with $\tilde{v}_{main} h/R$ (Figure 9). Then the measured secondary flow intensity appears to be considerably larger than the predicted one, which is in accordance with the results of the plane bed experiments (de Vriend and Koch, 1977), as shown by Figure 10*).
An explanation of this discrepancy between the measured and the predicted secondary flow intensity could possibly be found in the assumed vertical distribution of the eddy viscosity, as was stated already in the report on the plane

---

* This figure also shows the normalized helical velocities resulting from the plane bed experiments to be spread over a much wider range than those resulting from the uneven bed data, due to the use of an improved version of the current velocity/direction meter during the uneven bed experiments (see Appendices A, B).

bed experiments. In addition, part of the differences can be explained from systematic errors in the elaborated measured data (de Vriend, 1978), but these errors are considerably smaller than the differences observed, in particular now that the most serious source of systematic errors, the trapezoidal integration rule used for the calculation of depth-averaged quantities, has been eliminated from the elaboration procedure (see Appendix C).

3.6 Water surface configuration and energy head

Measured water surface elevations are presented in Table IV and energy heads in Table V.
In Figure 11 the measured water surface configuration is compared with the computed one, from which the conclusion can be drawn that the measured fall of the water level has been fairly well predicted, especially at the higher discharge (see Figure 11). The agreement between the longitudinal slopes of the energy head seems to be even better (Figure 12), but it should be noted that the scales in this figure are different from those in Figure 11.

The transverse configurations of the water surface (Figure 13) show a considerable discrepancy, in particular in the bend. The computed water surface elevation is too high in the outer part of the bend and too low in the inner part, and in the channel axis the transverse slope is much larger than the slope following from the measured data. In the direction perpendicular to the streamlines of the depth-averaged flow field the slope of the water surface must be proportional to $\bar{v}_{tot}^2/R_s$, when R_s denotes the radius of curvature of the streamline in the point considered (de Vriend, 1976 and 1977). Hence the water surface elevation must increase in radial direction, at least in regions where the streamlines are almost parallel to the channel axis. The computed elevations, however, show an outward decrease near the outer wall, from which it must be concluded that the computed transverse configuration of the water surface is in error.
The explanation of this error can be found in the computation method adopted: not the differential equations for the water surface elevation but those for the energy head have been integrated, and subsequently the water level was derived from the energy head. The deviation $z_s-\bar{z}_s$ of the water level from its mean value in the relevant cross-section, however, amounts to only a few percents of the energy head. So a small error in the energy head, due to numerical inaccuracies in the integration procedure, for instance, may have an important effect on the quantity $z_s-\bar{z}_s$. This explanation is confirmed by Figure 14, showing the transverse configuration of the energy head. The deviations of the computed distributions of

$e-\bar{e}$ from the measured ones can be explained by the deviations of the mean velocities, at least for the greater part.

The water level calculation can be improved either by increasing the accuracy of the energy head calculations (by reducing the mesh size, which is rather expensive, or by adopting a higher order integration rule), or by integrating the equations for z_s instead of those for e.

In the plane bed case, the computed transverse configuration of the water surface agreed much better with the measured ones than in the present case. This must be attributed to the much smaller variation of the mean velocity, and so of e, giving rise to much smaller variations of the integration error in e and hence to much smaller errors in $z_s-\bar{z}_s$.

4 Conclusions

1 The use of the improved type current velocity/direction meter (see Appendix A) leads to an important reduction of the scatter in the measured helical velocities.

2 In verticals belonging to the same class of Chézy factors, the distributions of the normalized main velocities are quite similar. In addition, the vertical distributions of the quantity $\frac{\kappa C}{\sqrt{g}}(v'_{main} - 1)$ in a cross-section hardly differ from one another, so that the main velocity can be concluded to allow a similarity approximation.

3 The normalized main velocity profiles resulting from the measurements show mostly small, but still significant, deviations from the logarithmic profile: in the lower part of a vertical the measured velocities are higher, in the upper part, and especially close to the water surface, they are lower than predicted by the logarithmic distribution. These differences occur throughout the flow and at both discharges, but they tend to be the largest in the bend and at the higher discharge.

4 In verticals belonging to the same class of Chézy factors, the distributions of the helical velocity component show great similarity. As, in addition, the measured data lie close to the theoretical curves to be derived from the logarithmic main velocity profile, it is concluded that the helical velocity component allows a similarity approximation in which the above-mentioned theoretical curves can serve to describe the vertical distribution.

5 The small counter-rotating secondary circulation found near the outer wall during the plane bed experiments (de Vriend and Koch, 1977) was not observed in the uneven bed case.

6 The predicted depth-averaged velocity field shows qualitatively the same deviations from the measured data as the plane bed case: the predicted shift of the velocity maximum towards the outer wall is too small. In spite of the great influence of the bed configuration on the mean velocity distribution, the deviations are not important.

7 The discrepancy between the measured and the computed mean velocity field must be attributed to the advective influence of the secondary flow on the main flow, which was not included in the mathematical model.

8 The intensity of the secondary flow was considerable only in the deeper parts of the bend, especially in cross-section C_o. As in the plane bed case, the predicted intensity in these deeper parts was about a factor 1.5 smaller than the measured one.

9 Regarding the discrepancy between the measured and the computed mean velocity distributions, the longitudinal configurations of the water surface and the energy head were rather well predicted.

10 The transverse configuration of the water surface and the energy head predicted by the mathematical model show much stronger deviations from the measured data than in the case of a plane bed, as a consequence of the much larger variations of the mean velocity.

REFERENCES

1 BROLSMA, P. (1973),
Temperature correction for micro propeller measurements (in Dutch),
Waterloopkundig Laboratorium, Informatie H 18, 1973.

2 DHL (1975),
Combined current-velocity/direction meter,
Delft Hydraulics Laboratory, Technical description, March 1975.

3 ENGELUND, F. (1974),
Flow and bed topography in channel bends,
Proceedings of the ASCE, Journal of the Hydraulics Division,
100, HY 11, November 1974, p. 1631.

4 KOCH, F.G. (1977),
Current direction meter investigation (in Dutch),
Waterloopkundig Laboratorium, Informatie R 657-VI, October 1977.

5 ROZOVSKII, I.L. (1961),
Flow of water in bends of open channels,
Israel Program for Scientific Translations, Jerusalem, 1961.

6 VRIEND, H.J. de (1976),
A mathematical model of steady flow in curved shallow channels,
Communications on Hydraulics, Dept. of Civil Engineering,
Delft University of Technology, Report 76-1, 1976.

7 VRIEND, H.J. de (1977),
A mathematical model of steady flow in curved shallow channels,
Journal of Hydraulic Research, 15 (1977), no. 1, pp. 37 - 54.

8 VRIEND, H.J. de (1978),
Accuracy of measurements in a curved open channel,
Delft Hydraulics Laboratory/Delft University of Technology,
TOW-report R 657-VII/M 1415, Part III, March 1978.

REFERENCES (continued)

9 VRIEND, H.J. de and KOCH, F.G. (1977),
Flow of water in a curved open channel with a fixed plane bed,
Delft Hydraulics Laboratory/Delft University of Technology,
TOW-report R 657-V/M 1415, Part I, October, 1977.

10 YEN, C.L. (1967),
Bed configuration and characteristics of subcritical flow in a meandering channel,
Ph.D. Thesis, University of Iowa, Iowa City, Iowa (USA), 1967.

11 YEN, C.L. (1970),
Bed topography effect on flow in a meander,
Proceedings of the ASCE, Journal of the Hydraulics Division,
96, HY 1, January 1970, p. 57.

tables

measurement serial number	discharge (m^3/s)	description	measurements	location
T5		inflow and outflow conditions		cross-section A_1
T5-1	0.463	inflow distribution	flow velocity	all verticals[2] 0.4 h above the bed
T5-2	0.463	influence shape tail gate	flow direction	cross-section E_0
T6		test series		
T6-1	0.463	accuracy of velocity measurements	flow velocity, 30 observations of 30 s duration	5 points in vertical D_0 4
T6-2	0.463	accuracy of direction measurements	flow direction, 30 observations of 270 s duration	4 points in verticals A_2 7 and D_0 4
T6-3	0.463	correlation of errors in velocity and direction measurements	flow velocity and direction, 30 observations of 60 s duration	3 points in vertical D_0 4
T7		vertical distribution of velocity (main flow and helical flow)	60 s average flow velocity and direction measured twice in each grid point[3]	verticals B_0 7, C_0 4, D_0 1, 4, 7, 10 and E_0 1, 4, 7, 10, 13
T7-1	0.463			
T7-2	0.232			
T8		total three-dimensional flow field	60 s average flow velocity and direction measured twice in each grid point[3]	all cross-sections[1] all verticals[2]
T8-1	0.463			
T8-2	0.232			
T9		horizontal distribution of water surface elevation	water surface elevation measured twice during measurements T7 and T8	all cross-sections[1] verticals 1, 3, 5, 7, 9, 11, 13
T9-1	0.462			
T9-2	0.232			

1) i.e. cross-sections A_1, A_2, B_0, B_1, C_0, C_1, D_0, D_1, E_0
2) i.e. verticals 1 to 13 incl.
3) see Section B.2.1 for a description of grid point locations

} see Figure 1

Table I Summary of measurements

section	0.463				0.232				Q (m^3/s)
	45-50	50-55	55-60	60-65	45-50	50-55	55-60	60-65	C ($m^{\frac{1}{2}}/s$)
	0.04-0.07	0.07-0.13	0.13-0.25	0.25-0.47	0.04-0.07	0.07-0.13	0.13-0.25	0.25-0.47	h (m)
A_1		1	2,3,4,5	6,7,8		1	2,3,4,5	6,7,8	
		13	9,10,11,12			13	9,10,11,12		
A_2		1	2,3,4,5	6,7,8		1	2,3,4,5	6,7,8	
		13	9,10,11,12			13	9,10,11,12		
B_0		1	2,3,4,5	6,7,8		1	2,3,4,5	6,7,8	
		13	9,10,11,12			13	9,10,11,12		
B_1		1	2	3,4,5,6		1	2	3.4.5,6	
		12,13	7,8,9,10,11			12,13	7,8,9,10,11		
C_0	12,13	10,11	1	2,3,4,5,6	12,13	10,11	1	2,3,4,5,6	
			7,8,9				7,8,9		
C_1	12,13	10,11	1	2,3,4,5,6	13	10,11,12	1	2,3,4,5,6	
			7,8,9				7,8,9		
D_0	12,13	10,11	1	2,3,4,5,6	13	10,11,12	1	2,3,4,5,6	
			7,8,9				7,8,9		
D_1	12,13	10,11	1	2,3,4,5,6	13	10,11,12	1	2,3,4,5,6	
			7,8,9				7,8,9		
E_0	13	10,11,12	1	2,3,4,5,6		10,11,12,13	1	2,3,4,5,6	
			7,8,9				7,8,9		

Table II Verticals grouped according to depth of flow and Chezy's factor

vert.	$\bar{v}_{tot}$ (m/s)	α (deg)	a_1	$\tilde{v}_{hel}$ (m/s)
1	0.230	0.0	0.0031	0.0007
2	0.303	0.3	0.0034	0.0010
3	0.380	0.4	0.0012	0.0005
4	0.410	0.7	0.0005	0.0002
5	0.428	0.6	0.0000	0.0000
6	0.445	0.2	0.0009	0.0004
7	0.446	-0.3	0.0014	0.0007
8	0.436	0.1	0.0014	0.0007
9	0.427	0.3	0.0007	0.0003
10	0.391	0.1	0.0000	0.0000
11	0.365	0.1	-0.0015	-0.0005
12	0.292	-0.1	-0.0029	-0.0008
13	0.240	0.3	-0.0013	-0.0003

Section A_1

vert.	$\bar{v}_{tot}$ (m/s)	α (deg)	a_1	$\tilde{v}_{hel}$ (m/s)
1	0.247	0.6	0.0030	0.0007
2	0.315	0.6	0.0025	0.0008
3	0.377	0.9	0.0007	0.0003
4	0.407	0.3	0.0012	0.0005
5	0.429	0.6	0.0002	0.0001
6	0.449	0.3	0.0006	0.0003
7	0.449	0.0	0.0006	0.0003
8	0.439	0.0	0.0000	0.0000
9	0.420	0.3	-0.0001	-0.0002
10	0.396	0.0	-0.0005	-0.0002
11	0.364	0.0	-0.0015	-0.0006
12	0.305	-0.1	-0.0023	-0.0007
13	0.246	-0.2	-0.0014	-0.0003

Section A_2

vert.	$\bar{v}_{tot}$ (m/s)	α (deg)	a_1	$\tilde{v}_{hel}$ (m/s)
1	0.227	-0.1	0.0034	0.0008
2	0.312	-0.6	0.0030	0.0010
3	0.366	-0.5	0.0024	0.0009
4	0.403	-0.4	0.0017	0.0008
5	0.431	0.3	0.0026	0.0011
6	0.444	-0.3	0.0004	0.0002
7	0.450	-0.7	0.0009	0.0004
8	0.443	-0.9	0.0007	0.0003
9	0.425	-0.6	0.0006	0.0002
10	0.403	-1.1	0.0002	0.0001
11	0.371	-0.8	-0.0003	-0.0001
12	0.323	-0.2	-0.0018	-0.0006
13	0.252	-0.2	-0.0022	-0.0006

Section B_0

vert.	$\bar{v}_{tot}$ (m/s)	α (deg)	a_1	$\tilde{v}_{hel}$ (m/s)
1	0.269	0.8	0.0078	0.0021
2	0.342	1.4	0.0007	0.0026
3	0.394	2.2	0.0074	0.0029
4	0.425	2.8	0.0071	0.0030
5	0.441	3.3	0.0062	0.0027
6	0.445	3.6	0.0055	0.0025
7	0.435	3.8	0.0044	0.0019
8	0.426	4.3	0.0035	0.0015
9	0.406	4.2	0.0033	0.0014
10	0.384	3.5	0.0025	0.0009
11	0.344	2.7	0.0028	0.0010
12	0.304	2.0	0.0022	0.0007
13	0.244	0.8	0.0014	0.0003

Section B_1

Table III Depth-averaged quantities (for reference see Appendix C)

a. $Q = 0.463\ m^3/s$

vert.	$\bar{v}_{tot}$ (m/s)	α (deg)	a_1	$\tilde{v}_{hel}$ (m/s)
1	0.365	0.5	0.0088	0.0033
2	0.410	0.6	0.0087	0.0036
3	0.442	0.7	0.0103	0.0046
4	0.449	0.8	0.0117	0.0053
5	0.446	1.2	0.0111	0.0050
6	0.427	0.7	0.0103	0.0044
7	0.406	0.9	0.0081	0.0033
8	0.375	1.2	0.0064	0.0024
9	0.345	1.5	0.0048	0.0017
10	0.308	1.4	0.0035	0.0011
11	0.273	1.7	0.0015	0.0004
12	0.228	1.1	0.0014	0.0003
13	0.191	0.7	0.0001	0.0000

Section C_0

vert.	$\bar{v}_{tot}$ (m/s)	α (deg)	a_1	$\tilde{v}_{hel}$ (m/s)
1	0.416	0.5	0.0058	0.0024
2	0.440	0.0	0.0066	0.0029
3	0.460	0.0	0.0081	0.0037
4	0.461	0.2	0.0096	0.0045
5	0.443	0.6	0.0103	0.0047
6	0.408	0.3	0.0091	0.0038
7	0.379	-0.1	0.0076	0.0029
8	0.350	0.0	0.0057	0.0020
9	0.310	0.1	0.0040	0.0012
10	0.266	-0.1	0.0026	0.0007
11	0.232	0.3	0.0011	0.0004
12	0.194	-0.1	0.0004	0.0001
13	0.168	-0.6	0.0017	0.0003

Section C_1

vert.	$\bar{v}_{tot}$ (m/s)	α (deg)	a_1	$\tilde{v}_{hel}$ (m/s)
1	0.420	0.6	0.0054	0.0022
2	0.445	-0.1	0.0067	0.0030
3	0.468	0.1	0.0070	0.0033
4	0.454	0.0	0.0089	0.0040
5	0.442	0.3	0.0106	0.0048
6	0.401	0.0	0.0093	0.0038
7	0.366	-0.2	0.0089	0.0030
8	0.334	-0.3	0.0068	0.0023
9	0.295	0.1	0.0043	0.0013
10	0.253	0.1	0.0024	0.0006
11	0.217	0.3	0.0009	0.0002
12	0.185	-0.2	0.0006	0.0001
13	0.163	-0.4	0.0000	0.0000

Section D_0

vert.	$\bar{v}_{tot}$ (m/s)	α (deg)	a_1	$\tilde{v}_{hel}$ (m/s)
1	0.424	0.7	0.0054	0.0019
2	0.450	0.3	0.0064	0.0029
3	0.452	0.2	0.0073	0.0033
4	0.449	0.4	0.0094	0.0042
5	0.427	0.5	0.0100	0.0043
6	0.395	-0.1	0.0098	0.0040
7	0.355	-0.3	0.0072	0.0026
8	0.321	-0.2	0.0064	0.0021
9	0.278	0.3	0.0041	0.0012
10	0.238	-0.4	0.0031	0.0008
11	0.203	-0.4	0.0020	0.0004
12	0.175	0.2	-0.0002	0.0000
13	0.156	-0.6	0.0025	0.0004

Section D_1

Table IIIa (continued)

vert.	$\bar{v}_{tot}$ (m/s)	α (deg)	a_1	$\tilde{v}_{hel}$ (m/s)
1	0.422	0.3	0.0046	0.0019
2	0.449	0.2	0.0057	0.0026
3	0.454	0.1	0.0076	0.0035
4	0.444	0.3	0.0094	0.0042
5	0.421	0.2	0.0103	0.0044
6	0.386	0.1	0.0099	0.0039
7	0.355	-0.4	0.0081	0.0029
8	0.304	-0.1	0.0057	0.0018
9	0.266	0.4	0.0048	0.0013
10	0.233	0.1	0.0031	0.0007
11	0.193	0.2	0.0025	0.0005
12	0.166	0.2	0.0001	0.0000
13	0.151	-0.8	0.0015	0.0002

Section E_0

Table IIIa (continued)

vert.	$\bar{v}_{tot}$ (m/s)	α (deg)	a_1	$\tilde{v}_{hel}$ (m/s)
1	0.106	0.7	0.0041	0.0004
2	0.141	0.9	0.0019	0.0003
3	0.176	0.8	0.0016	0.0003
4	0.194	0.7	-0.0007	-0.0001
5	0.205	0.5	-0.0001	0.0000
6	0.214	0.1	0.0001	0.0000
7	0.220	-0.2	0.0012	0.0003
8	0.227	-0.3	0.0004	0.0001
9	0.208	0.2	-0.0001	0.0000
10	0.135	-0.3	-0.0001	0.0000
11	0.163	-0.1	-0.0022	-0.0004
12	0.136	0.1	-0.0025	-0.0003
13	0.111	0.9	-0.0017	-0.0002

Section A_1

vert.	$\bar{v}_{tot}$ (m/s)	α (deg)	a_1	$\tilde{v}_{hel}$ (m/s)
1	0.112	0.7	0.0013	0.0001
2	0.145	0.7	0.0023	0.0003
3	0.177	0.7	0.0007	0.0001
4	0.194	0.4	0.0004	0.0001
5	0.208	0.7	-0.0001	0.0000
6	0.218	0.2	0.0006	0.0001
7	0.216	-0.1	0.0001	0.0000
8	0.212	0.1	-0.0009	-0.0002
9	0.203	0.3	-0.0007	-0.0001
10	0.189	0.0	-0.0023	-0.0004
11	0.165	0.1	-0.0021	-0.0003
12	0.140	0.1	-0.0020	-0.0003
13	0.109	0.2	-0.0017	-0.0002

Section A_2

vert.	$\bar{v}_{tot}$ (m/s)	α (deg)	a_1	$\tilde{v}_{hel}$ (m/s)
1	0.107	-0.4	0.0038	0.0004
2	0.143	-0.6	0.0032	0.0005
3	0.170	-0.7	0.0017	0.0003
4	0.189	-0.6	0.0012	0.0002
5	0.202	-0.3	0.0005	0.0001
6	0.212	-0.5	0.0004	0.0001
7	0.213	-0.6	0.0007	0.0002
8	0.211	-0.9	0.0004	0.0001
9	0.204	-0.8	0.0005	0.0001
10	0.188	-1.0	-0.0002	-0.0001
11	0.171	-0.7	-0.0010	-0.0002
12	0.148	-0.2	-0.0021	-0.0003
13	0.114	-0.1	-0.0031	-0.0004

Section B_0

vert.	$\bar{v}_{tot}$ (m/s)	α (deg)	a_1	$\tilde{v}_{hel}$ (m/s)
1	0.121	0.7	0.0068	0.0008
2	0.157	1.1	0.0073	0.0012
3	0.182	1.8	0.0075	0.0014
4	0.199	2.3	0.0065	0.0013
5	0.212	3.2	0.0060	0.0013
6	0.214	3.5	0.0054	0.0011
7	0.208	3.7	0.0043	0.0009
8	0.204	3.9	0.0028	0.0006
9	0.191	2.1	0.0149	0.0028
10	0.180	2.9	0.0024	0.0004
11	0.161	2.3	0.0022	0.0003
12	0.138	1.6	0.0004	0.0001
13	0.111	0.6	-0.0014	-0.0002

Section B_1

Table III Depth-averaged quantities (for reference see Appendix C)

b. $Q = 0.232\ m^3/s$

vert.	$\bar{v}_{tot}$ (m/s)	α (deg)	a_1	$\tilde{v}_{hel}$ (m/s)
1	0.165	0.6	0.0081	0.0013
2	0.187	0.2	0.0093	0.0018
3	0.204	0.8	0.0099	0.0021
4	0.210	0.8	0.0112	0.0024
5	0.207	0.9	0.0108	0.0023
6	0.198	0.9	0.0093	0.0019
7	0.187	0.9	0.0074	0.0014
8	0.173	1.3	0.0063	0.0011
9	0.155	1.5	0.0042	0.0007
10	0.137	1.4	0.0028	0.0004
11	0.132	1.7	0.0018	0.0002
12	0.102	1.2	0.0012	0.0001
13	0.078	0.6	0.0016	0.0001

Section C_0

vert.	$\bar{v}_{tot}$ (m/s)	α (deg)	a_1	$\tilde{v}_{hel}$ (m/s)
1	0.189	0.3	0.0051	0.0009
2	0.205	-0.2	0.0063	0.0013
3	0.214	0.0	0.0079	0.0017
4	0.211	-0.1	0.0097	0.0021
5	0.203	0.0	0.0101	0.0021
6	0.189	-0.1	0.0087	0.0017
7	0.175	0.0	0.0068	0.0012
8	0.159	0.0	0.0054	0.0009
9	0.139	0.2	0.0032	0.0005
10	0.122	0.4	0.0023	0.0003
11	0.104	0.1	0.0008	0.0001
12	0.089	0.0	0.0020	0.0002
13	0.079	-0.2	0.0027	0.0002

Section C_1

vert.	$\bar{v}_{tot}$ (m/s)	α (deg)	a_1	$\tilde{v}_{hel}$ (m/s)
1	0.195	0.5	0.0045	0.0009
2	0.208	-0.2	0.0059	0.0013
3	0.216	0.0	0.0072	0.0016
4	0.210	0.0	0.0093	0.0020
5	0.199	0.2	0.0101	0.0021
6	0.184	-0.1	0.0090	0.0017
7	0.167	0.0	0.0064	0.0011
8	0.150	-0.4	0.0056	0.0009
9	0.131	-0.4	0.0043	0.0006
10	0.114	0.1	0.0017	0.0002
11	0.098	0.4	0.0011	0.0001
12	0.0085	0.1	0.0017	0.0001
13	0.076	-0.1	0.0001	0.0000

Section D_0

vert.	$\bar{v}_{tot}$ (m/s)	α (deg)	a_1	$\tilde{v}_{hel}$ (m/s)
1	0.198	0.4	0.0045	0.0009
2	0.210	0.1	0.0061	0.0013
3	0.214	-0.1	0.0076	0.0016
4	0.207	0.2	0.0096	0.0020
5	0.196	0.2	0.0107	0.0021
6	0.179	0.0	0.0097	0.0018
7	0.161	-0.1	0.0076	0.0012
8	0.142	0.3	0.0053	0.0008
9	0.124	0.2	0.0035	0.0004
10	0.108	0.0	0.0017	0.0002
11	0.095	-0.1	0.0015	0.0001
12	0.084	0.0	0.0006	0.0001
13	0.076	0.5	-0.0007	0.0000

Section D_1

Table IIIb (continued)

vert.	$\bar{v}_{tot}$ (m/s)	α (deg)	a_1	$\tilde{v}_{hel}$ (m/s)
1	0.199	0.6	0.0033	0.0006
2	0.211	0.0	0.0061	0.0013
3	0.211	0.1	0.0079	0.0017
4	0.203	0.2	0.0094	0.0020
5	0.190	0.2	0.0105	0.0020
6	0.174	-0.3	0.0102	0.0018
7	0.155	-0.6	0.0077	0.0012
8	0.138	0.2	0.0055	0.0008
9	0.119	0.3	0.0036	0.0004
10	0.106	0.4	0.0023	0.0003
11	0.091	0.7	0.0011	0.0001
12	0.080	0.5	0.0010	0.0001
13	0.074	0.9	0.0009	0.0001

Section E_0

Table IIIb (continued)

vert.	cross-section								
	A_1	A_2	B_0	B_1	C_0	C_1	D_0	D_1	E_0
1	0.2540	0.2520	0.2501	0.2482	0.2469	0.2447	0.2428	0.2409	0.2393
3	0.2539	0.2519	0.2498	0.2476	0.2465	0.2441	0.2425	0.2406	0.2391
5	0.2539	0.2518	0.2497	0.2474	0.2459	0.2437	0.2422	0.2402	0.2388
7	0.2539	0.2518	0.2496	0.2469	0.2455	0.2435	0.2419	0.2401	0.2384
9	0.2536	0.2520	0.2494	0.2468	0.2452	0.2433	0.2417	0.2399	0.2384
11	0.2536	0.2519	0.2495	0.2464	0.2448	0.2424	0.2414	0.2398	0.2381
13	0.2536	0.2418	0.2491	0.2462	0.2447	0.2429	0.2413	0.2396	0.2381

Table IV Water surface elevations (m)

a. Q = 0.463 m/s

vert.	cross-section								
	A_1	A_2	B_0	B_i	C_0	C_1	D_0	D_1	E_0
1	0.2508	0.2505	0.2501	0.2493	0.2491	0.2488	0.2474	0.2471	0.2468
3	0.2507	0.2503	0.2499	0.2492	0.2489	0.2485	0.2474	0.2470	0.2467
5	0.2506	0.2502	0.2497	0.2489	0.2482	0.2481	0.2474	0.2469	0.2467
7	0.2506	0.2502	0.2497	0.2486	0.2481	0.2483	0.2473	0.2469	0.2466
9	0.2505	0.2501	0.2497	0.2498	0.2486	0.2483	0.2475	0.2472	0.2470
11	0.2506	0.2501	0.2496	0.2488	0.2485	0.2481	0.2473	0.2463	0.2467
13	0.2504	0.2500	0.2495	0.2483	0.2483	0.2481	0.2472	0.2469	0.2466

Table IV Water surface elevation (m)

b. Q = 0.232 m/s

vert.		cross-section							
	A_1	A_2	B_0	B_1	C_0	C_1	D_0	D_1	E_0
1	0.2567	0.2551	0.2527	0.2519	0.2537	0.2535	0.2518	0.2501	0.2482
3	0.2613	0.2591	0.2566	0.2535	0.2565	0.2551	0.2537	0.2510	0.2496
5	0.2532	0.2612	0.2592	0.2574	0.2560	0.2537	0.2522	0.2495	0.2478
7	0.2640	0.2621	0.2572	0.2572	0.2539	0.2508	0.2487	0.2465	0.2448
9	0.2629	0.2610	0.2586	0.2552	0.2513	0.2482	0.2461	0.2438	0.2420
11	0.2604	0.2587	0.2565	0.2524	0.2486	0.2451	0.2438	0.2419	0.2400
13	0.2565	0.2549	0.2523	0.2492	0.2466	0.2443	0.2427	0.2408	0.2393

Table V Energy head (m)

a. $Q = 0.463\ m^3/s$

vert.	cross-section								
	A_1	A_2	B_0	B_1	C_0	C_1	D_0	D_1	E_0
1	0.2514	0.2511	0.2507	0.2500	0.2505	0.2506	0.2493	0.2491	0.2488
3	0.2523	0.2519	0.2509	0.2509	0.2510	0.2508	0.2498	0.2493	0.2490
5	0.2527	0.2524	0.2518	0.2512	0.2504	0.2502	0.2494	0.2498	0.2485
7	0.2531	0.2526	0.2520	0.2508	0.2499	0.2499	0.2487	0.2482	0.2478
9	0.2527	0.2522	0.2518	0.2508	0.2497	0.2493	0.2484	0.2480	0.2477
11	0.2520	0.2515	0.2511	0.2501	0.2494	0.2487	0.2478	0.2468	0.2471
13	0.2510	0.2506	0.2502	0.2489	0.2486	0.2484	0.2475	0.2472	0.2469

Table V Energy head

b. $Q = 0.232\ m^3/s$

figures

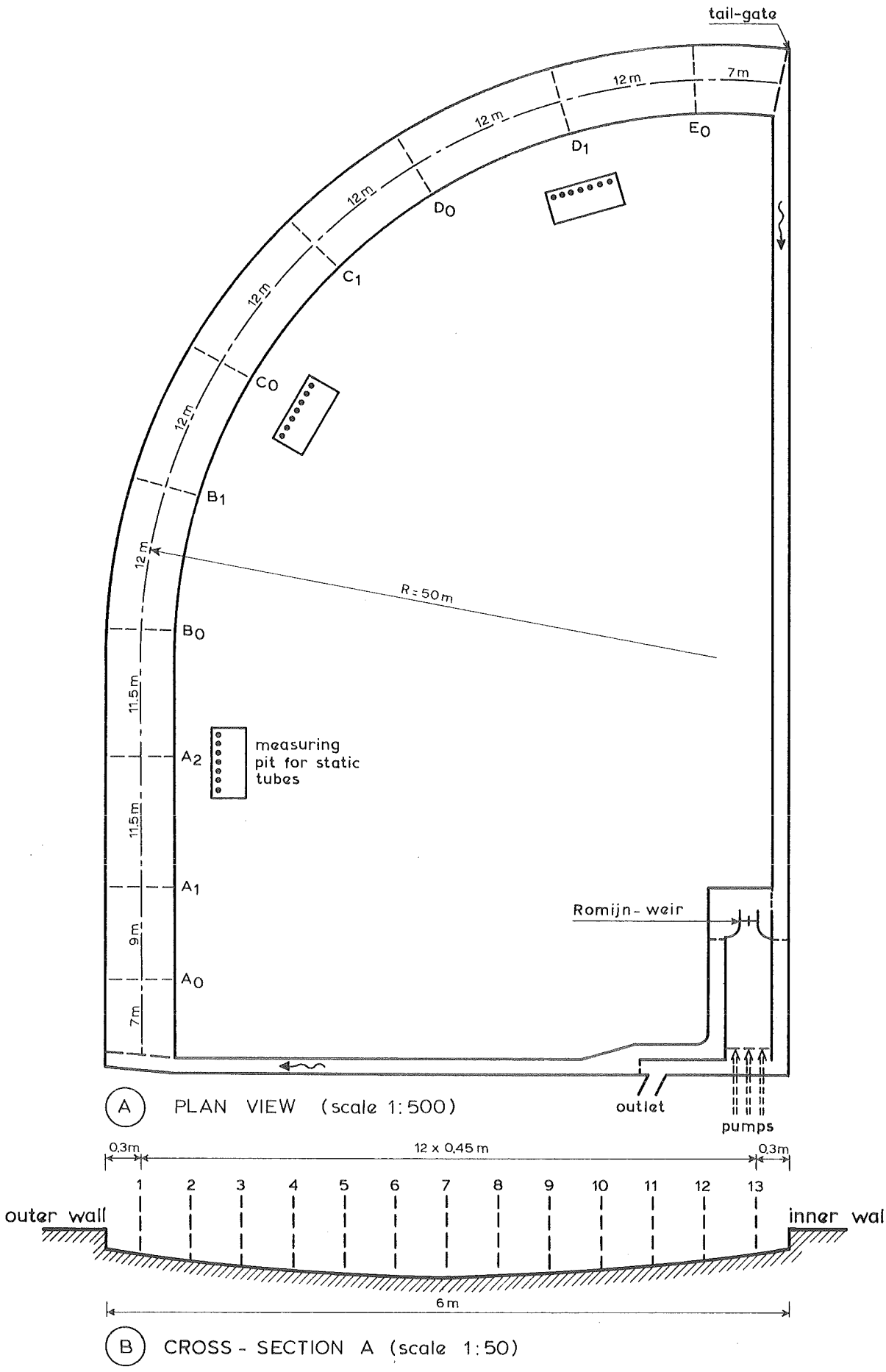

CHANNEL GEOMETRY

DELFT HYDRAULICS LABORATORY/DELFT UNIVERSITY OF TECHNOLOGY | R657/M1415 | FIG. 1

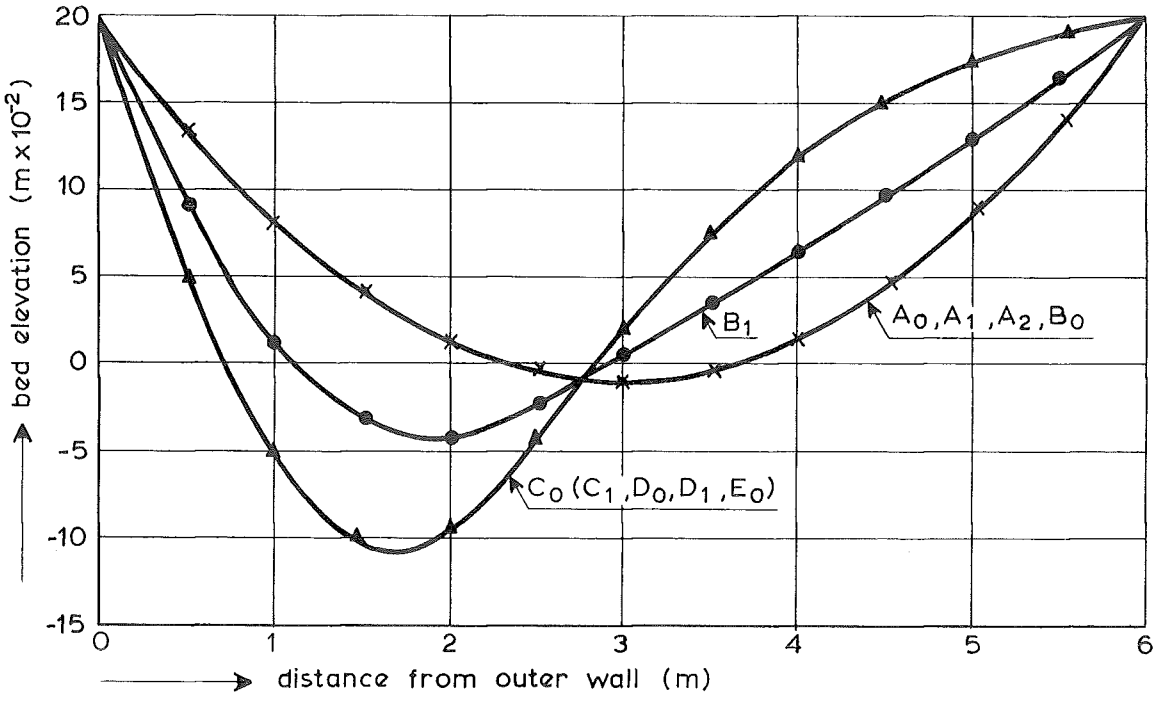

Ⓐ CROSS-SECTIONS

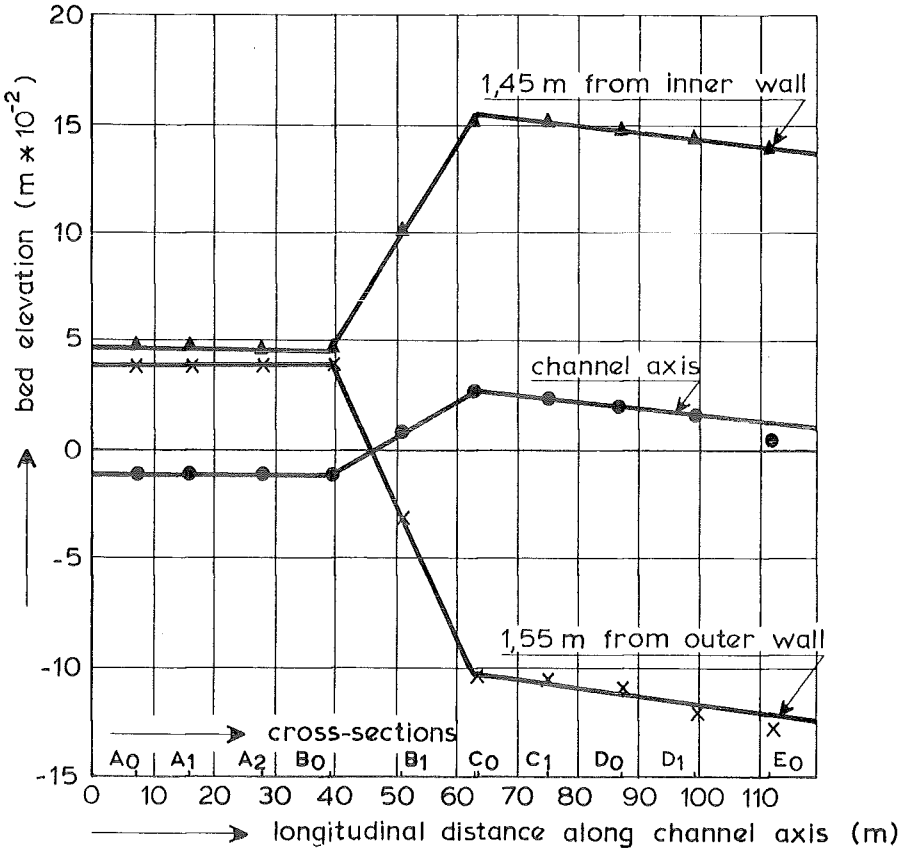

Ⓑ LONGITUDINAL SECTIONS

BED ELEVATION		
DELFT HYDRAULICS LABORATORY/DELFT UNIVERSITY OF TECHNOLOGY	R657/M1415	FIG. 2

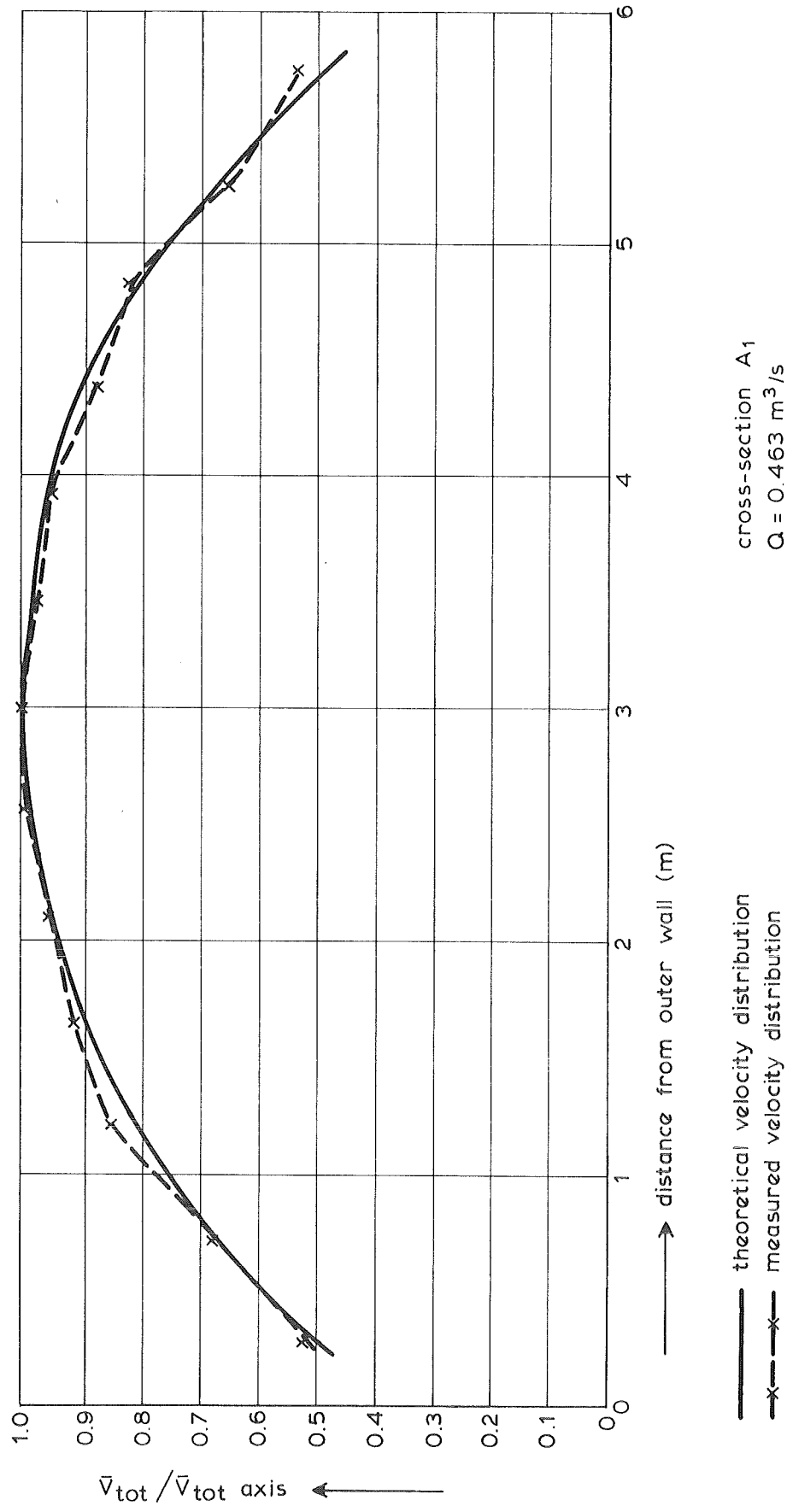

DEPTH-AVERAGED INFLOW VELOCITY DISTRIBUTION	T 5-1	
DELFT HYDRAULICS LABORATORY/ DELFT UNIVERSITY OF TECHNOLOGY	R657/M1415	FIG. 3

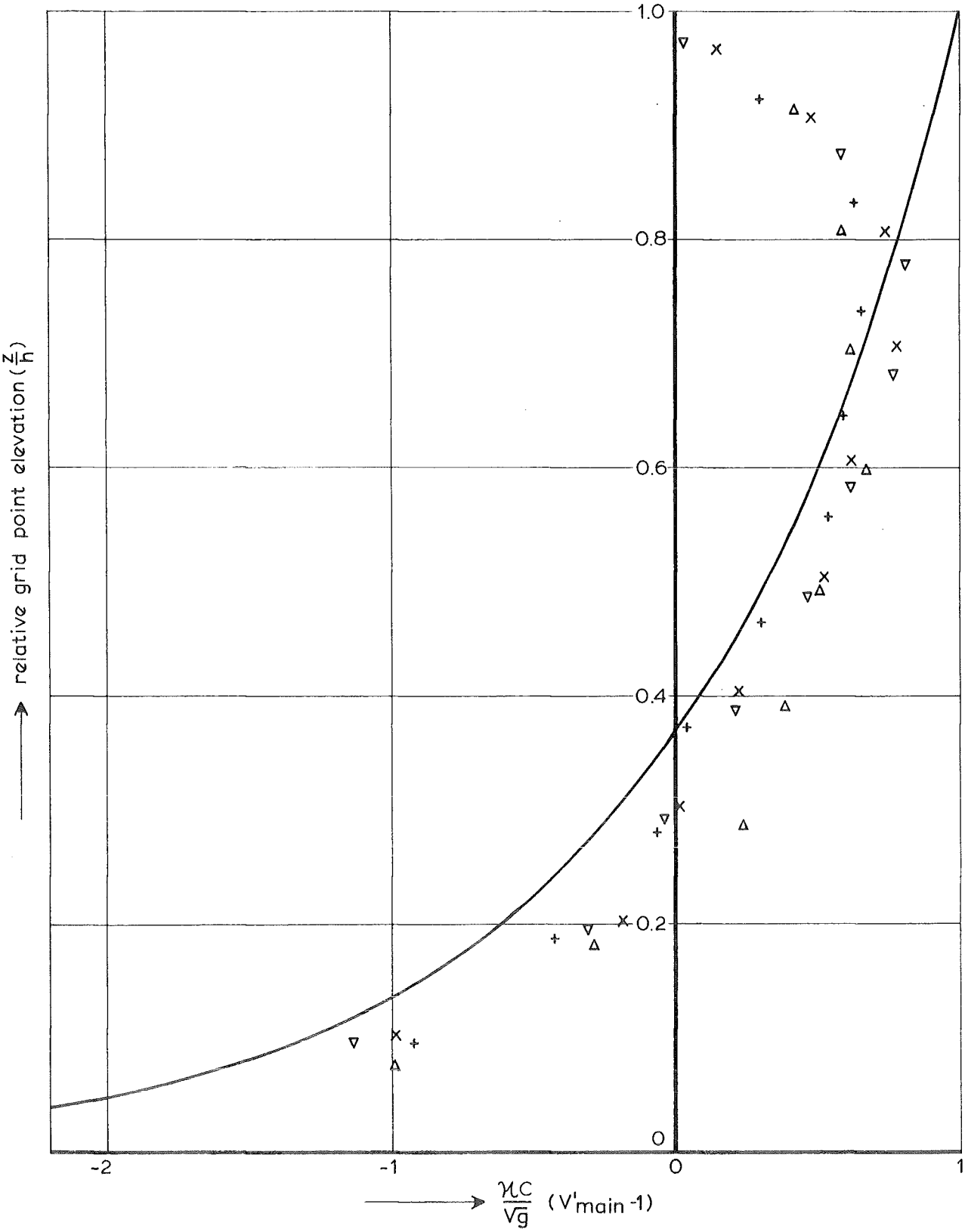

+ vertical B_o 7 } uneven bed ($Q = 0.463\ m^3/s$)
Δ " D_o 4 }
× " B_o 7 } plane bed ($Q = 0.61\ m^3/s$)
▽ " D_o 4 }
——— theory

MAIN VELOCITY PROFILES COMPARED WITH PLANE BED DATA

T 2-1, T 7-1

DELFT HYDRAULICS LABORATORY/DELFT UNIVERSITY OF TECHNOLOGY | R657/M1415 | FIG. 6

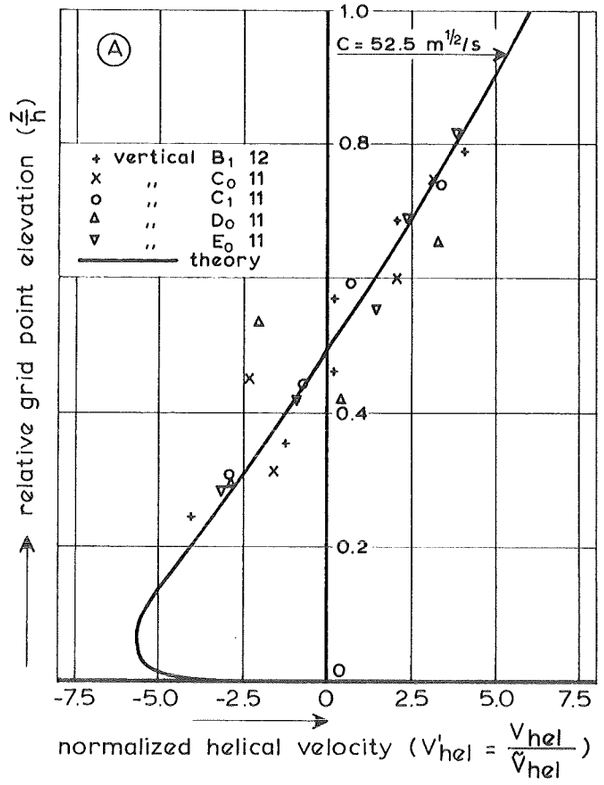

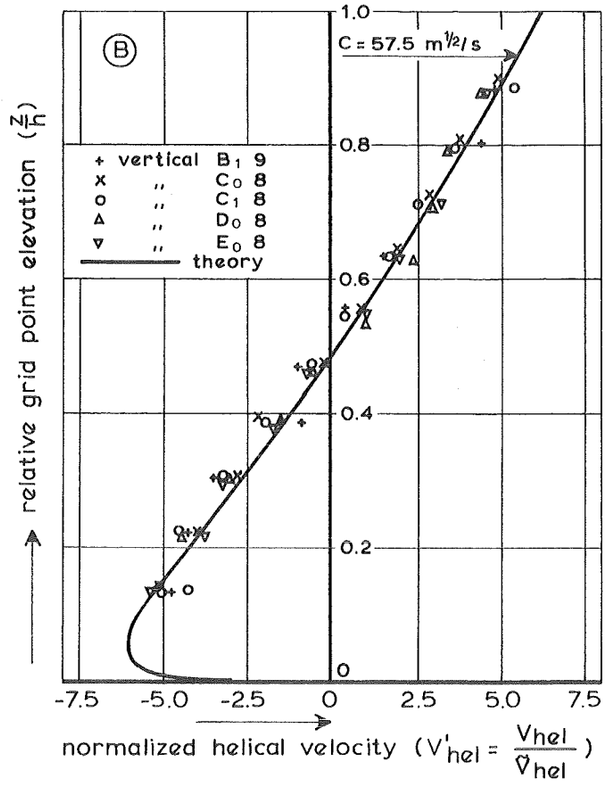

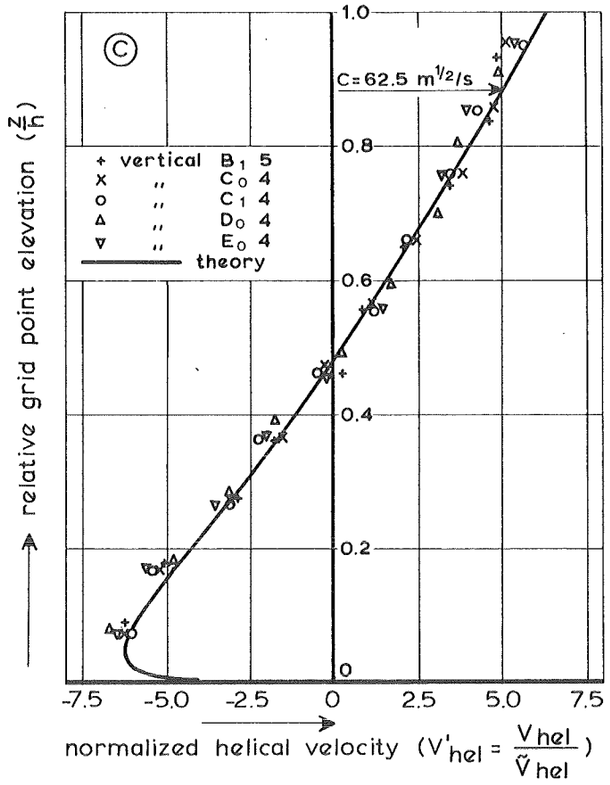

T 8-1
Q = 0.463 m³/s

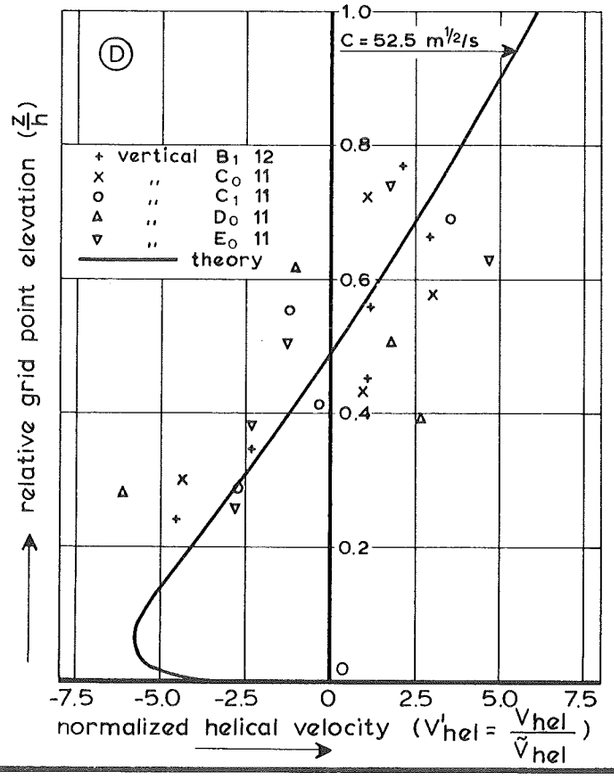

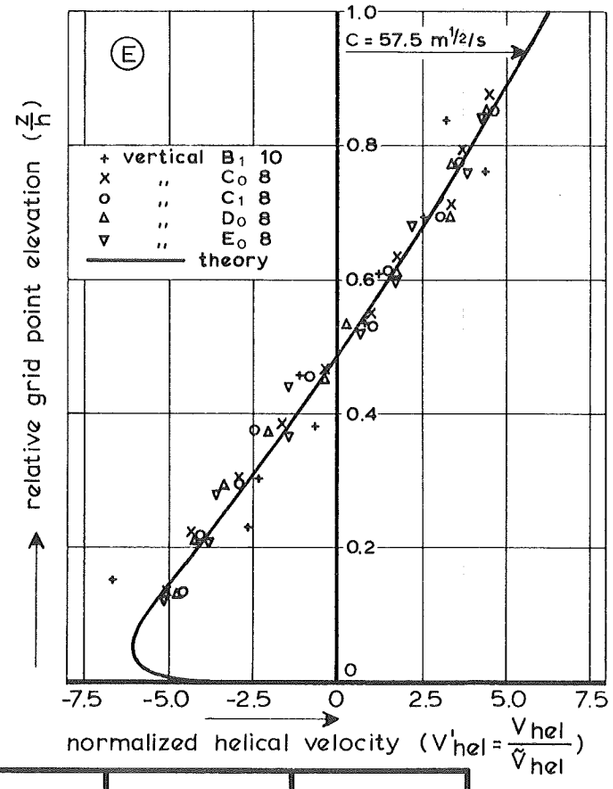

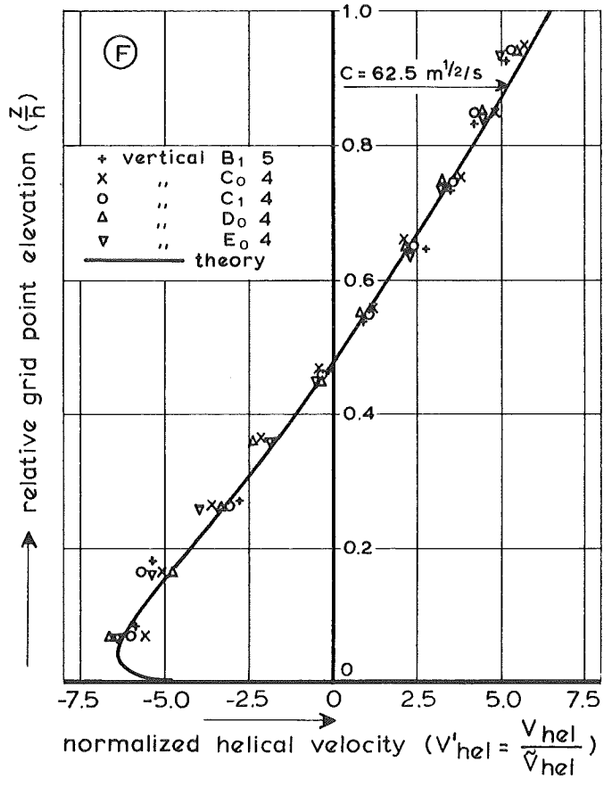

T 8-2
Q = 0.232 m³/s

SIMILARITY OF THE VERTICAL DISTRIBUTION OF THE HELICAL VELOCITY

T8 - 1, 2

DELFT HYDRAULICS LABORATORY/DELFT UNIVERSITY OF TECHNOLOGY | R657/M1415 | FIG. 7

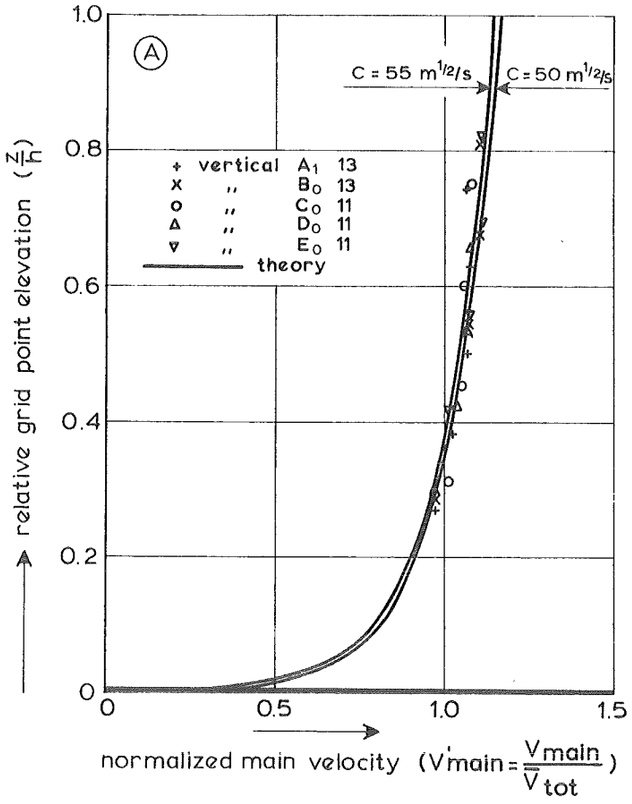

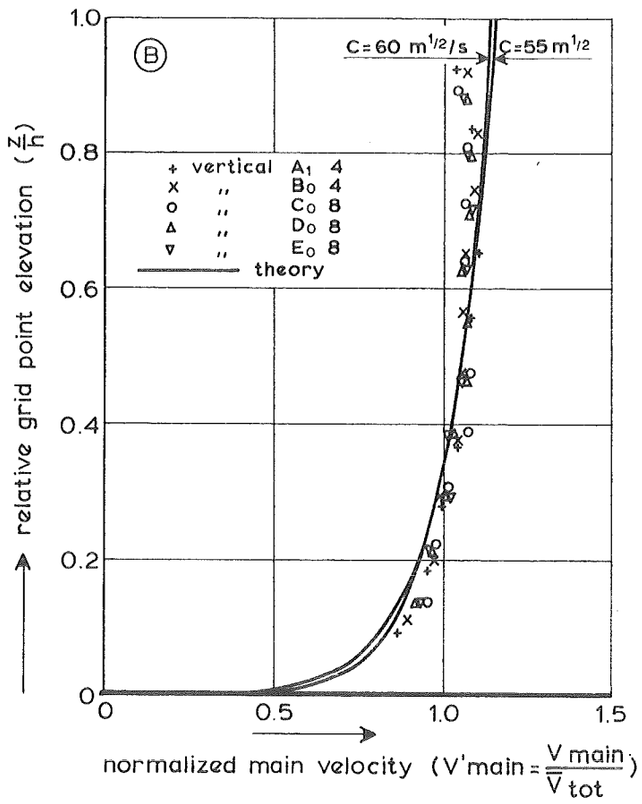

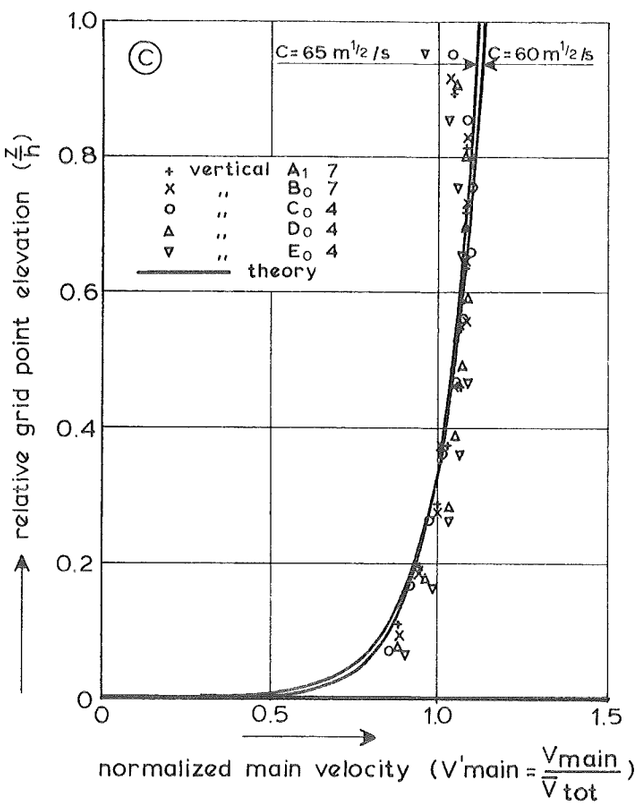

T 8-1
Q = 0.463 m³/s

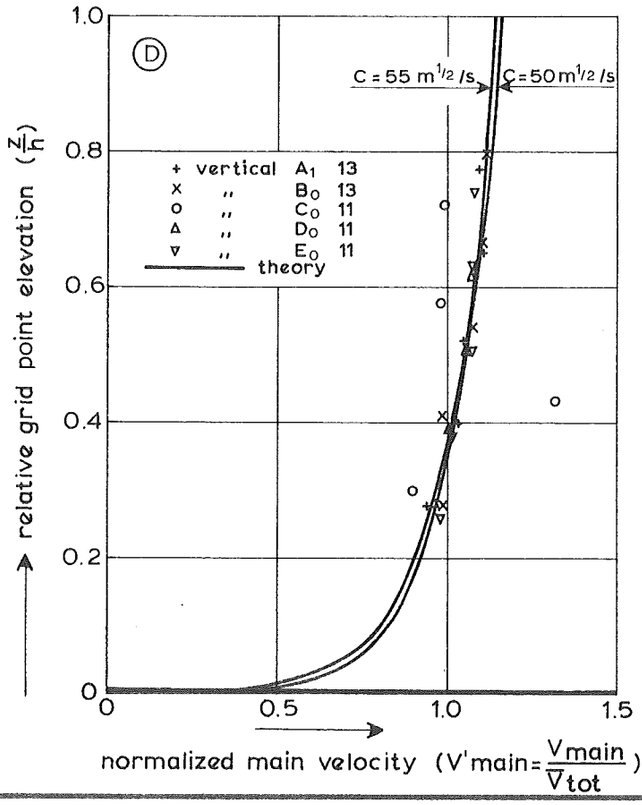

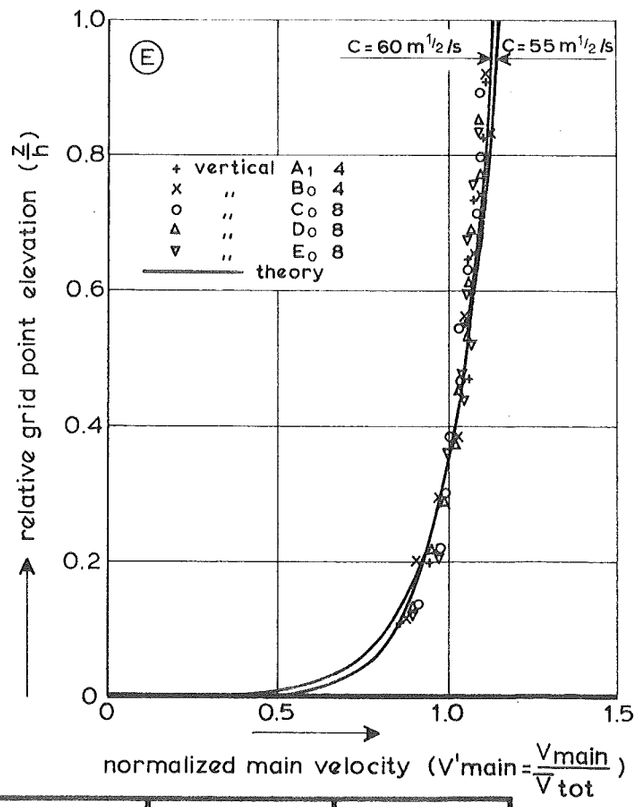

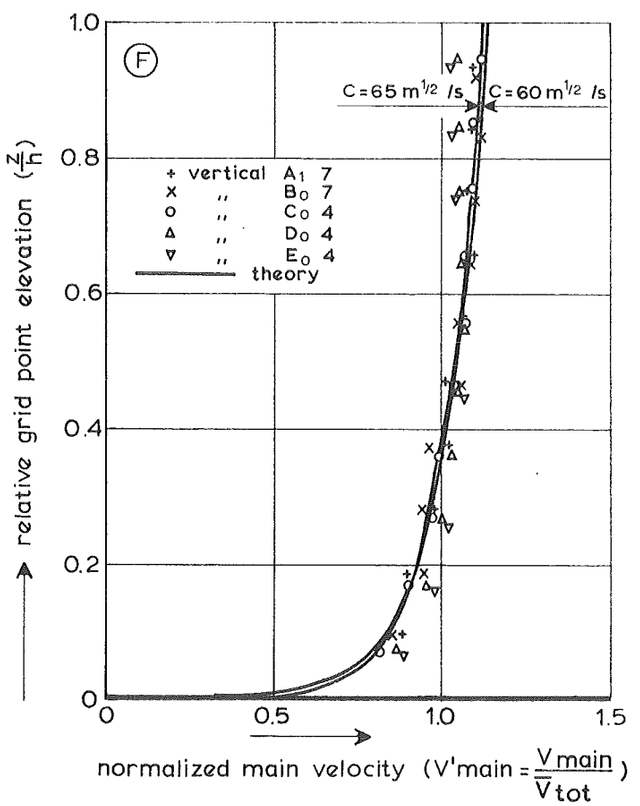

T 8-2
Q = 0.232 m³/s

SIMILARITY OF THE VERTICAL DISTRIBUTION OF THE MAIN VELOCITY	T 8-1,2	
DELFT HYDRAULICS LABORATORY/DELFT UNIVERSITY OF TECHNOLOGY	R657/M1415	FIG. 4

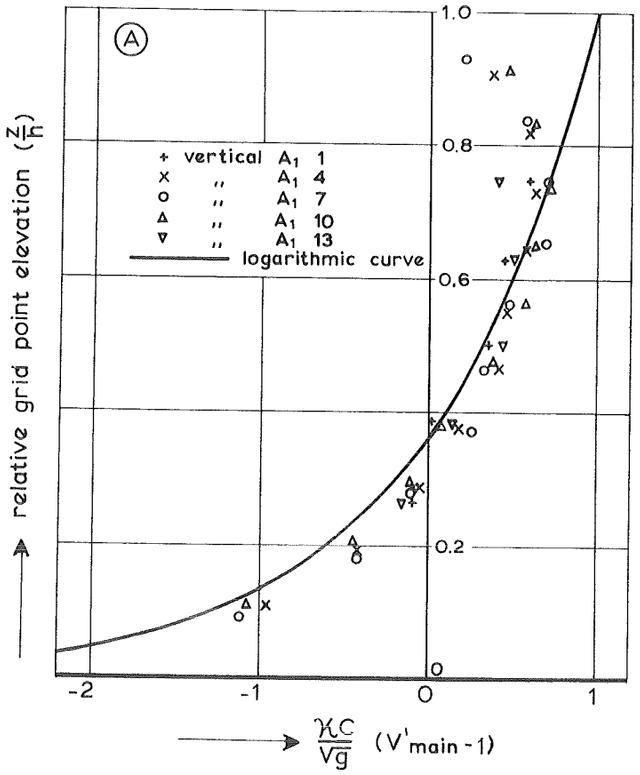

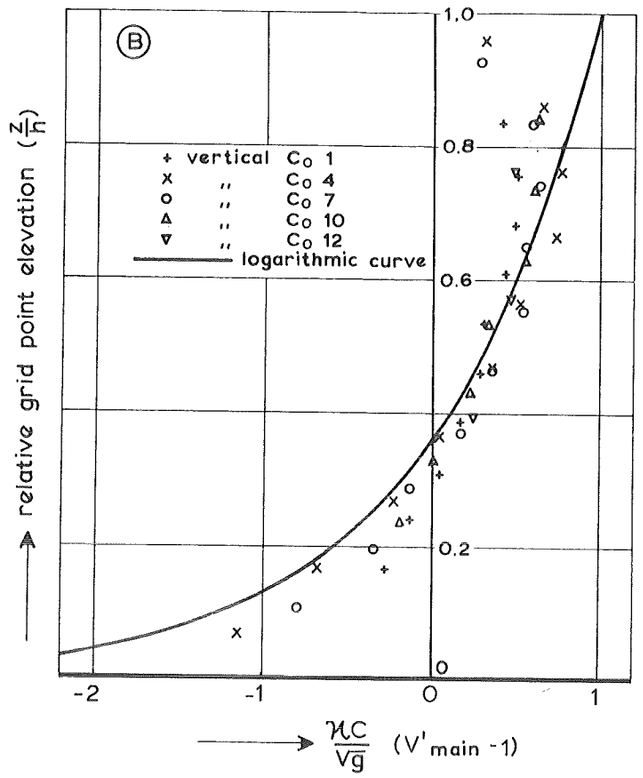

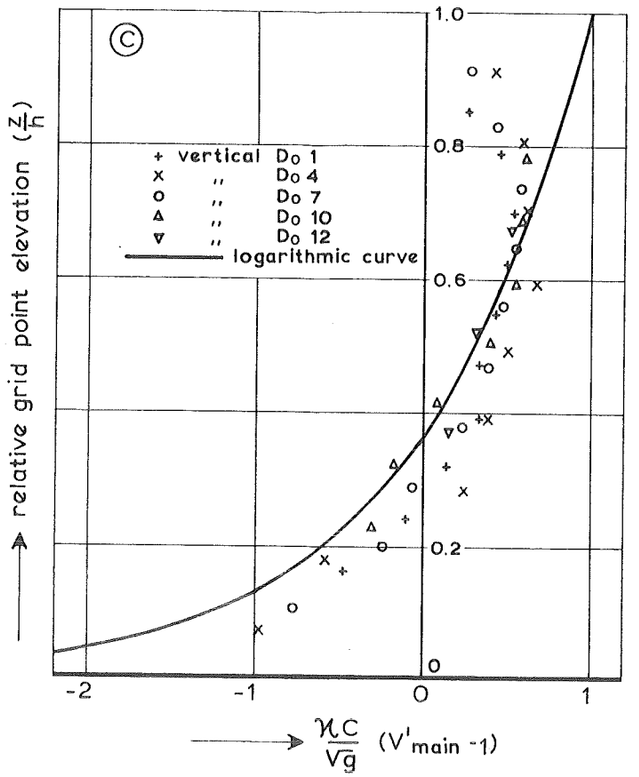

T 8-1
Q = 0.463 m³/s

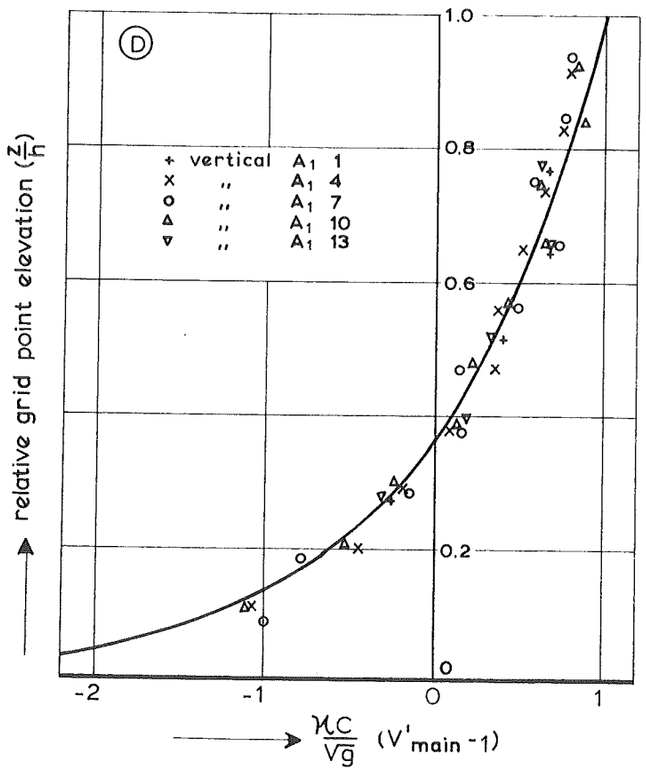

T 8 - 2
Q = 0.232 m³/s

APPLICABILITY OF THE LOGARITHMIC MAIN VELOCITY PROFILE	T 8 - 1,2	
DELFT HYDRAULICS LABORATORY / DELFT UNIVERSITY OF TECHNOLOGY	R657/M1415	FIG. 5

COMPARISON BETWEEN THE DEPTH AVERAGED VELOCITIES

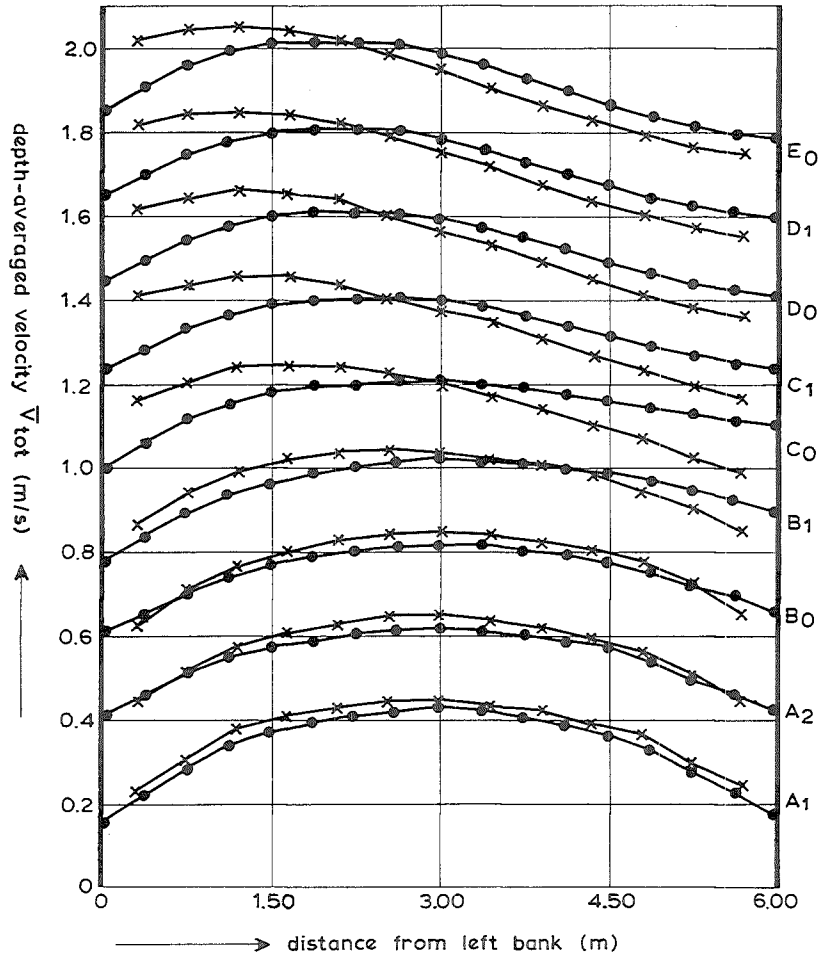

Ⓐ Q = 0.463 m³/s

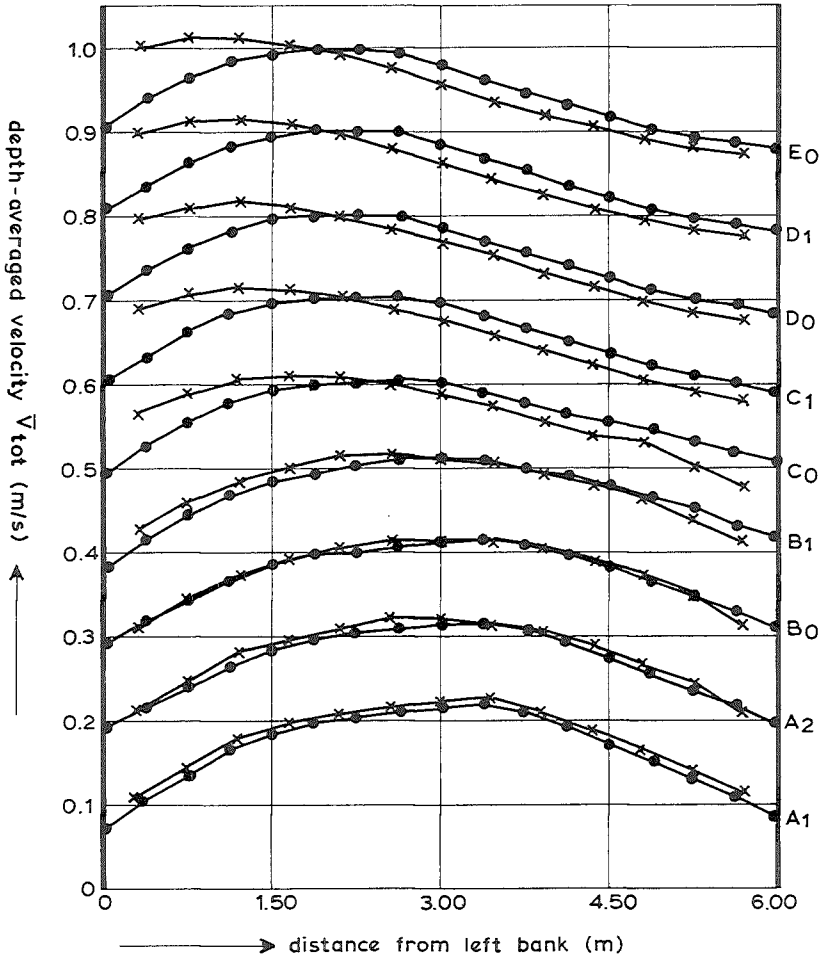

Ⓑ Q = 0.232 m³/s

theory

measured

Ⓐ The velocity scale is given for section A_1; in the subsequent sections $\bar{V}_{tot}$ has been raised by 0.2 m/s every time

Ⓑ The velocity scale is given for section A_1; in the subsequent sections $\bar{V}_{tot}$ has been raised by 0.1 m/s every time

DELFT HYDRAULICS LABORATORY/DELFT UNIVERSITY OF TECHNOLOGY
R657/M1415
FIG. 8

COMPARISON BETWEEN INTENSITIES OF THE SECONDARY FLOW

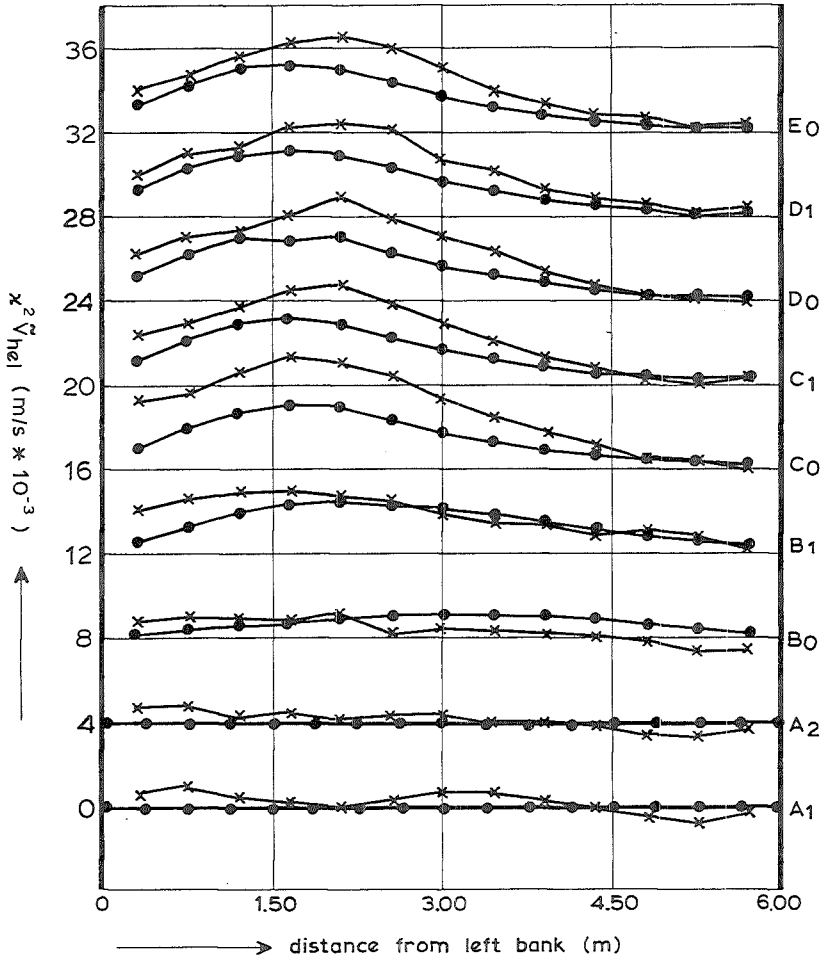

Ⓐ Q = 0.463 m^3/s

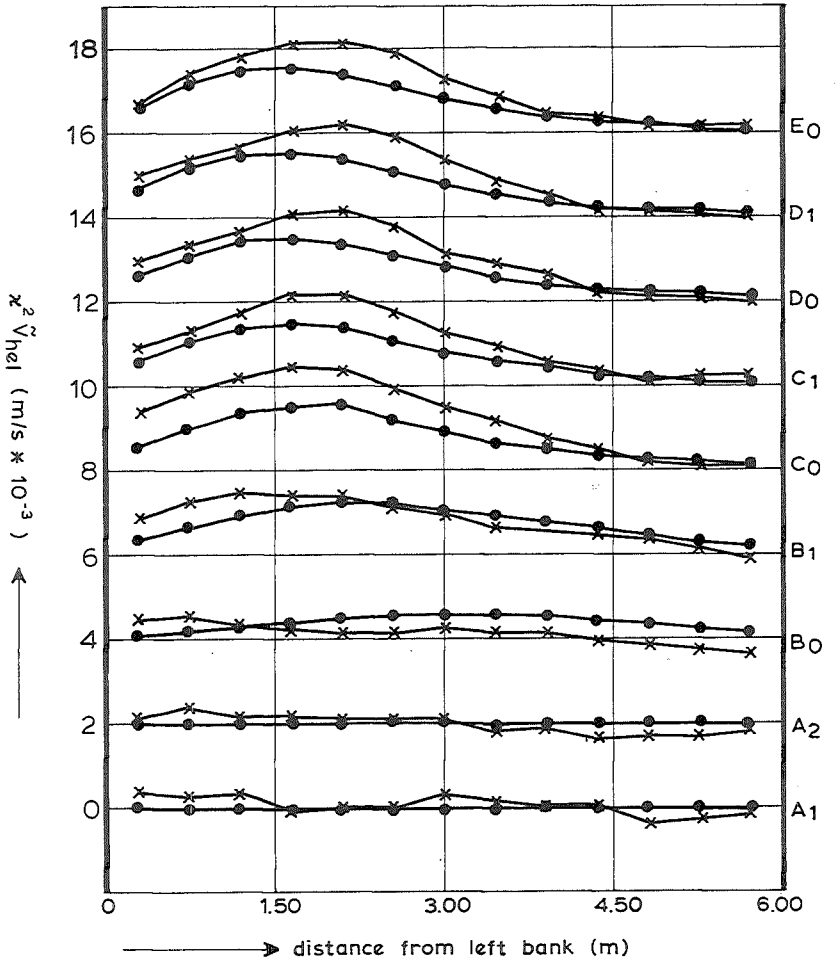

Ⓑ Q = 0.232 m^3/s

$\frac{\tilde{V} \text{ main } h}{R}$

measured

Ⓐ The velocity scale is given for section A_1; in the subsequent sections $x^2 \tilde{V}_{hel}$ has been raised by $4 * 10^{-3}$ m/s every time

Ⓑ The velocity scale is given for section A_1; in the subsequent sections $x^2 \tilde{V}_{hel}$ has been raised by $2 * 10^{-3}$ m/s every time

DELFT HYDRAULICS LABORATORY / DELFT UNIVERSITY OF TECHNOLOGY

R657/M1415 FIG. 9

T 8 - 1,2

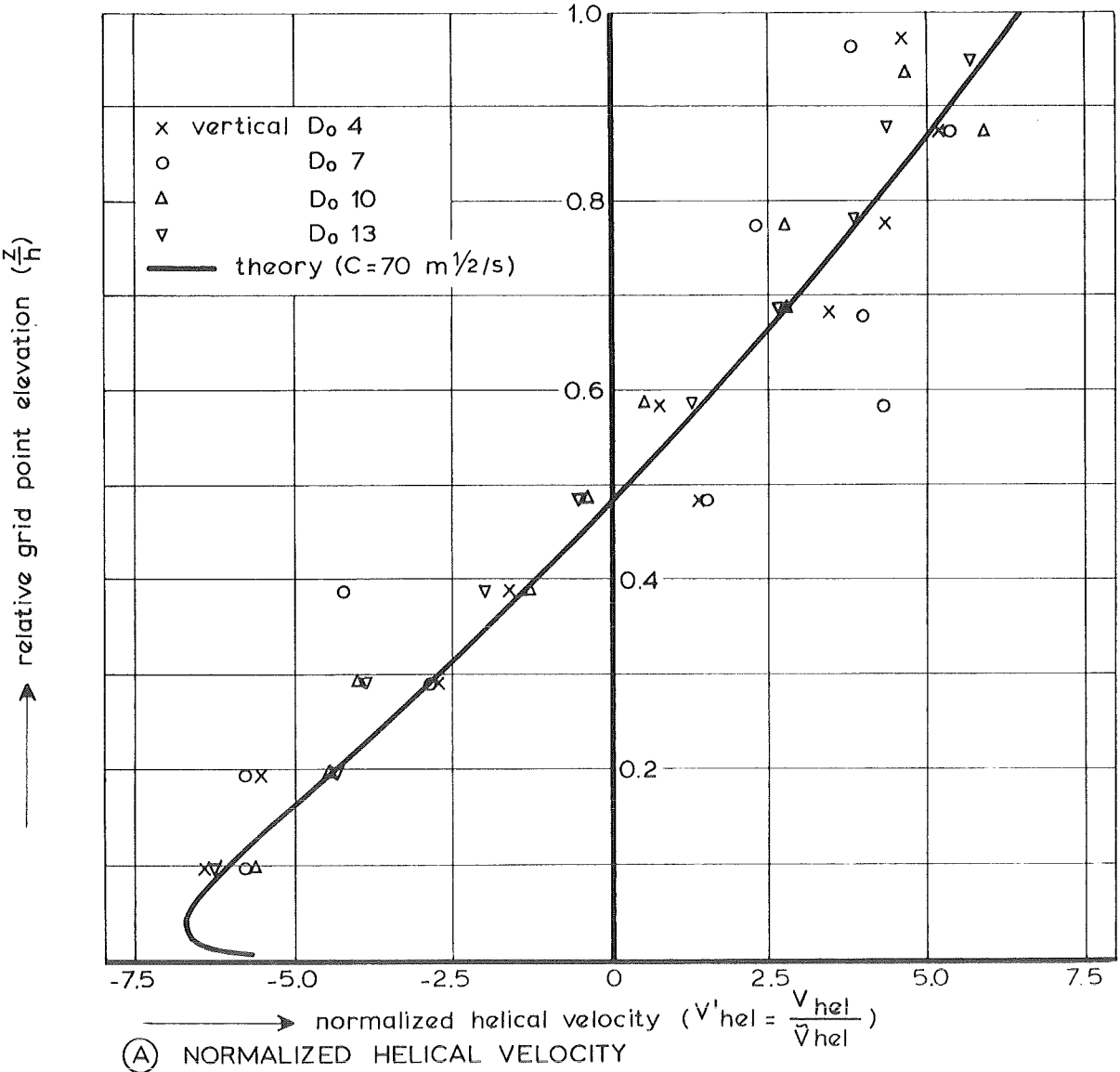

(A) NORMALIZED HELICAL VELOCITY

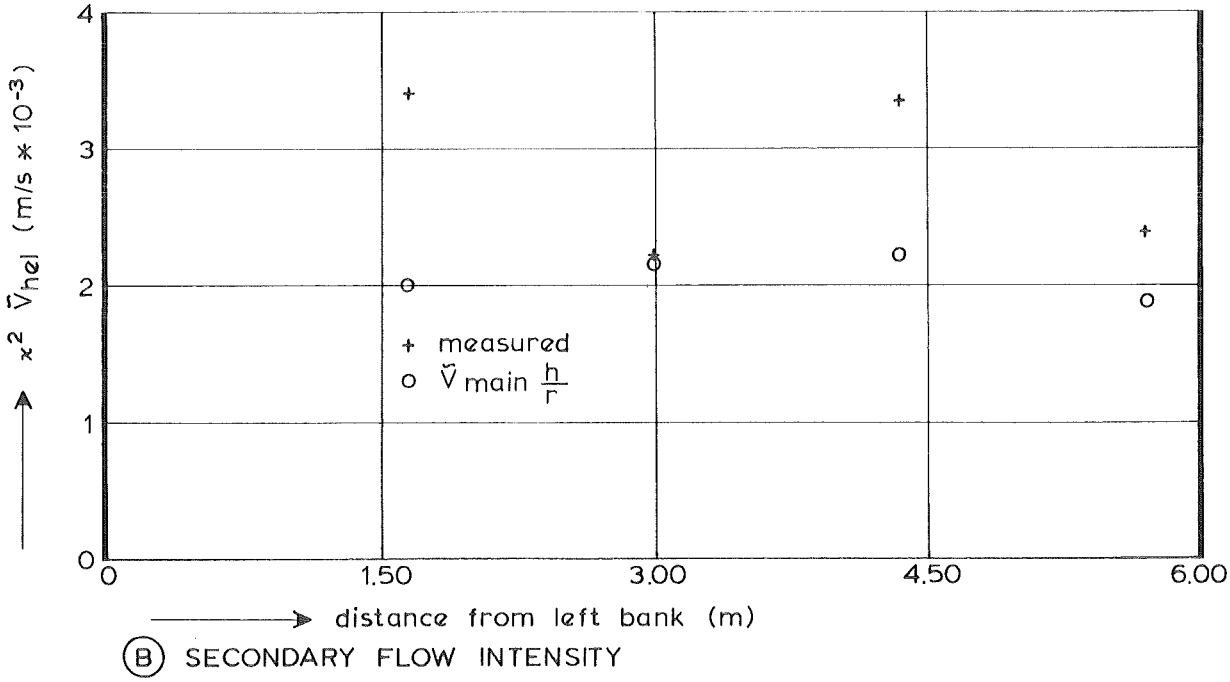

(B) SECONDARY FLOW INTENSITY

SECONDARY FLOW IN SECTION D_0 (PLANE BED)	T 2-1	
DELFT HYDRAULICS LABORATORY/DELFT UNIVERSITY OF TECHNOLOGY	R657/M1415	FIG. 10

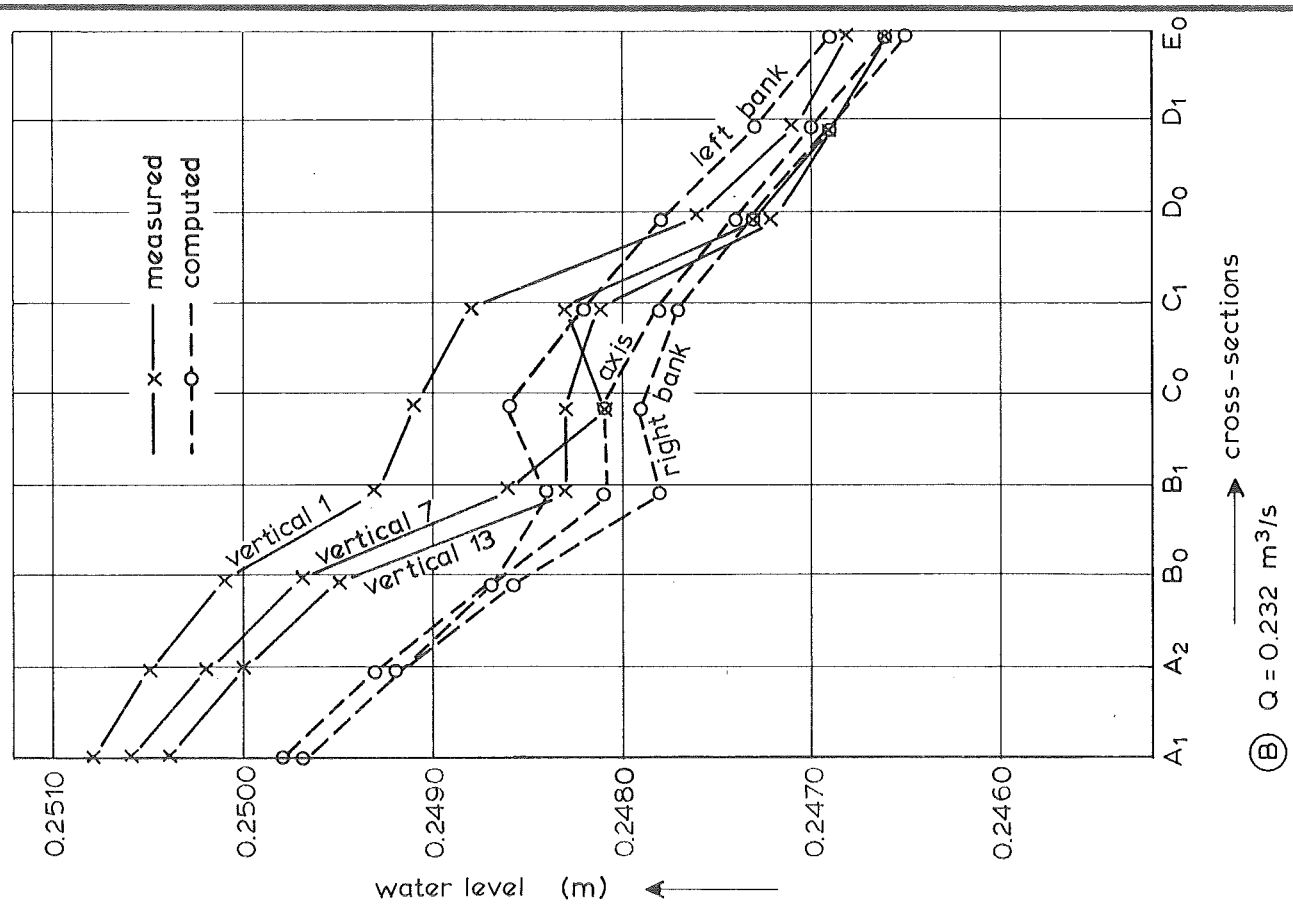

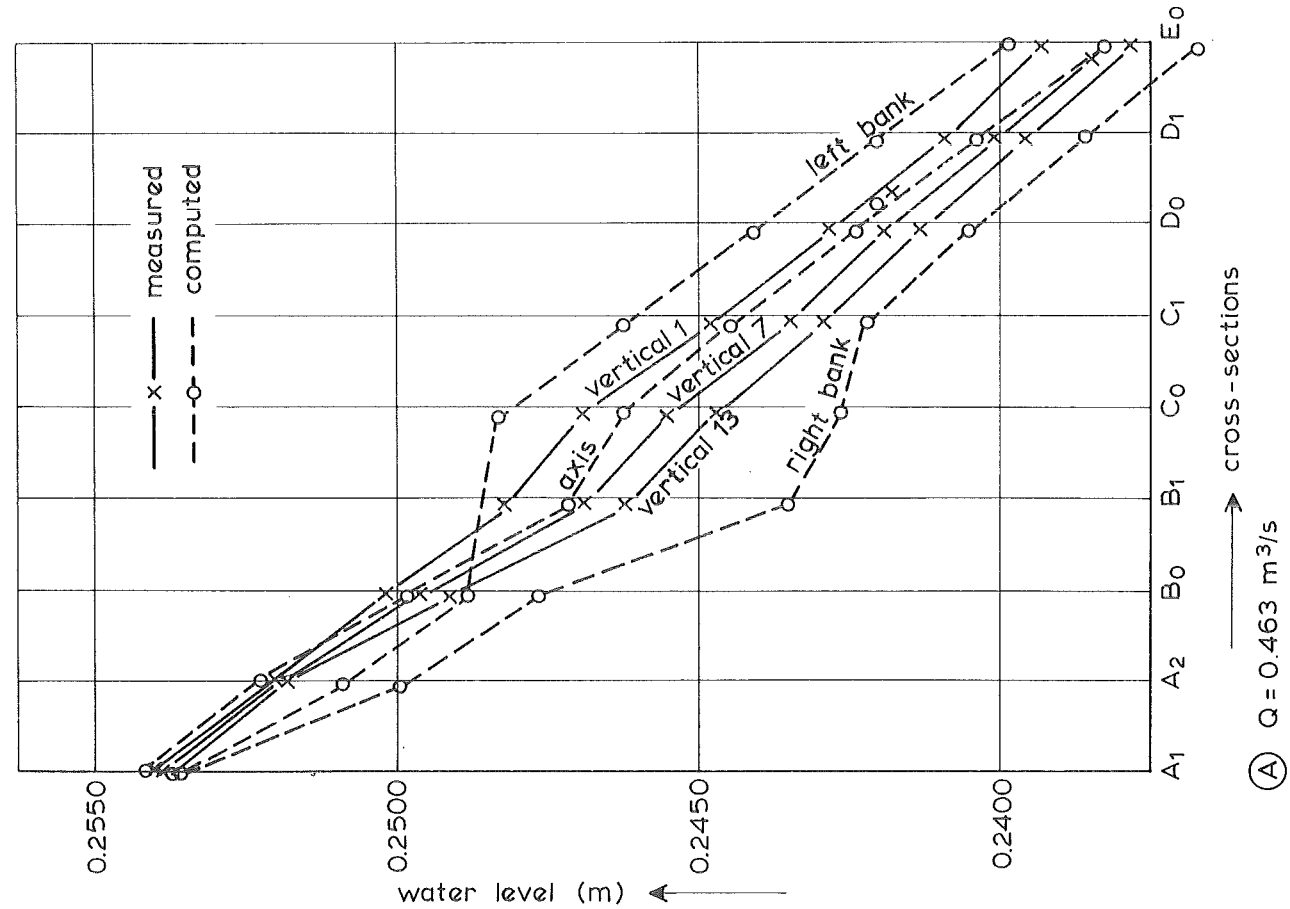

WATER SURFACE ELEVATION

T 9 - 1,2

DELFT HYDRAULICS LABORATORY / DELFT UNIVERSITY OF TECHNOLOGY | R657/M1415 | FIG. 11

T9 - 834

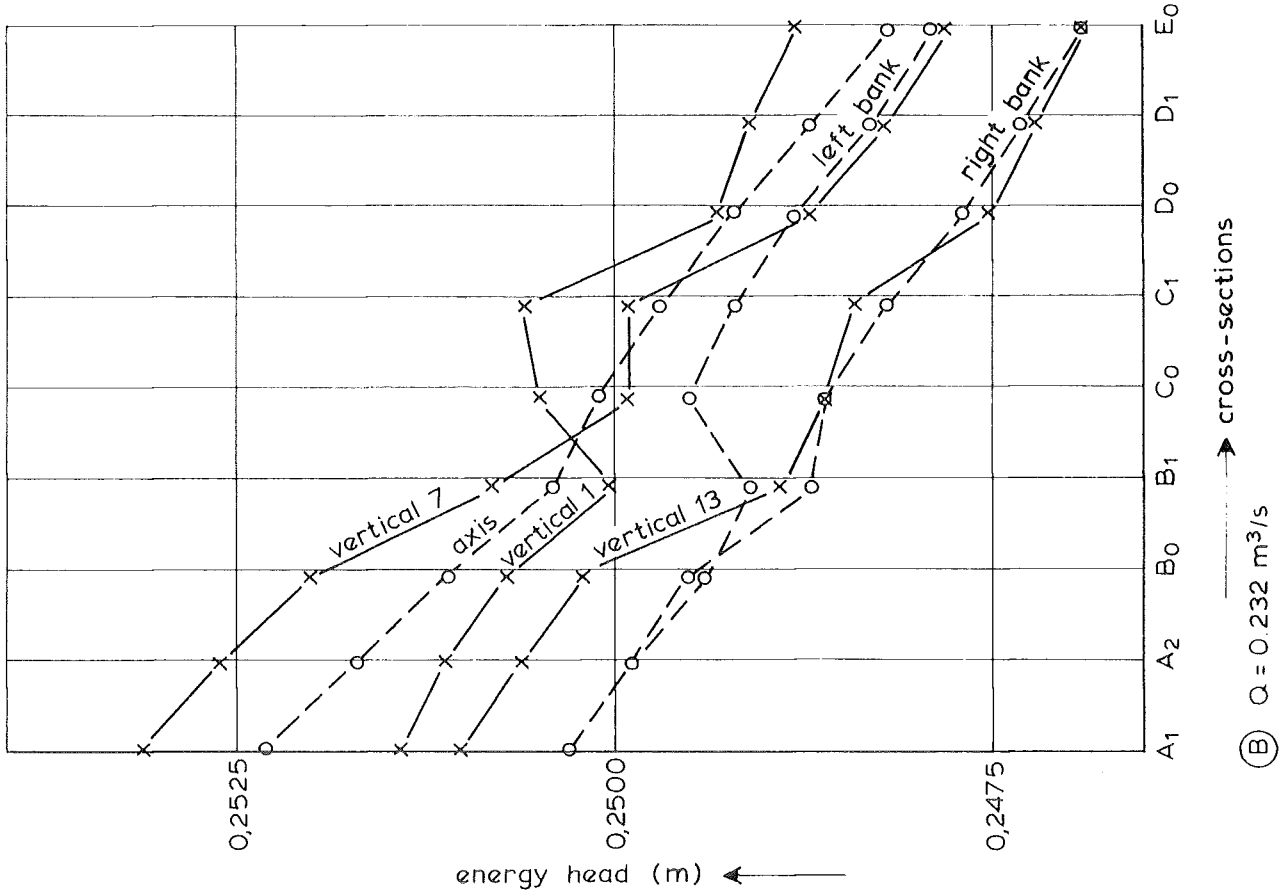

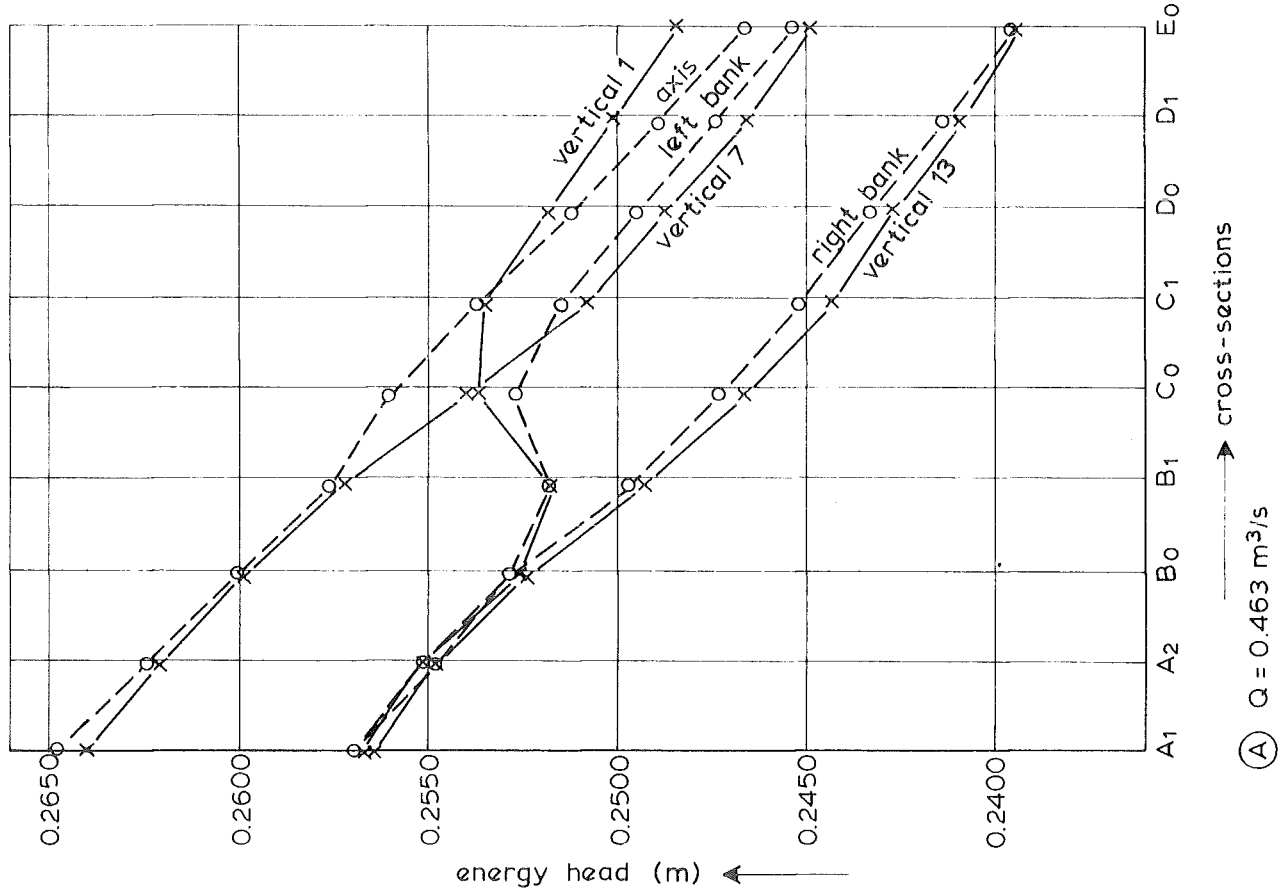

ENERGY HEAD

T 9 - 1,2

DELFT HYDRAULICS LABORATORY/DELFT UNIVERSITY OF TECHNOLOGY | R657/M1415 | FIG. 12

TRANSVERSE CONFIGURATION OF THE WATER SURFACE

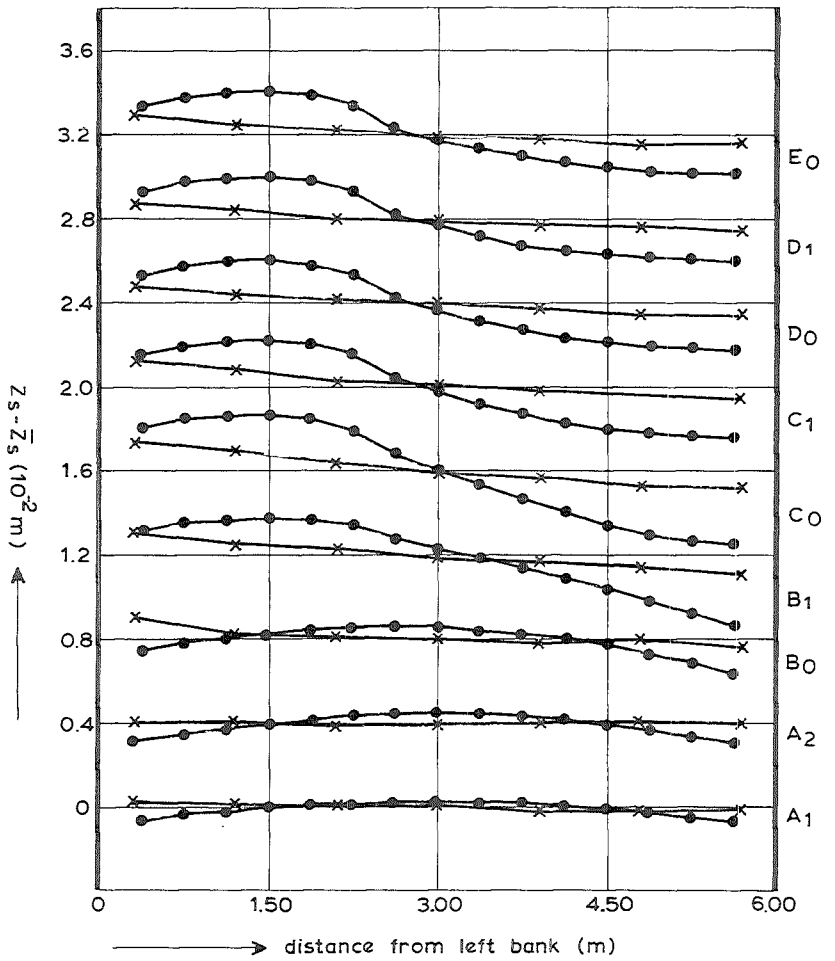

Ⓐ Q = 0.463 m^3/s

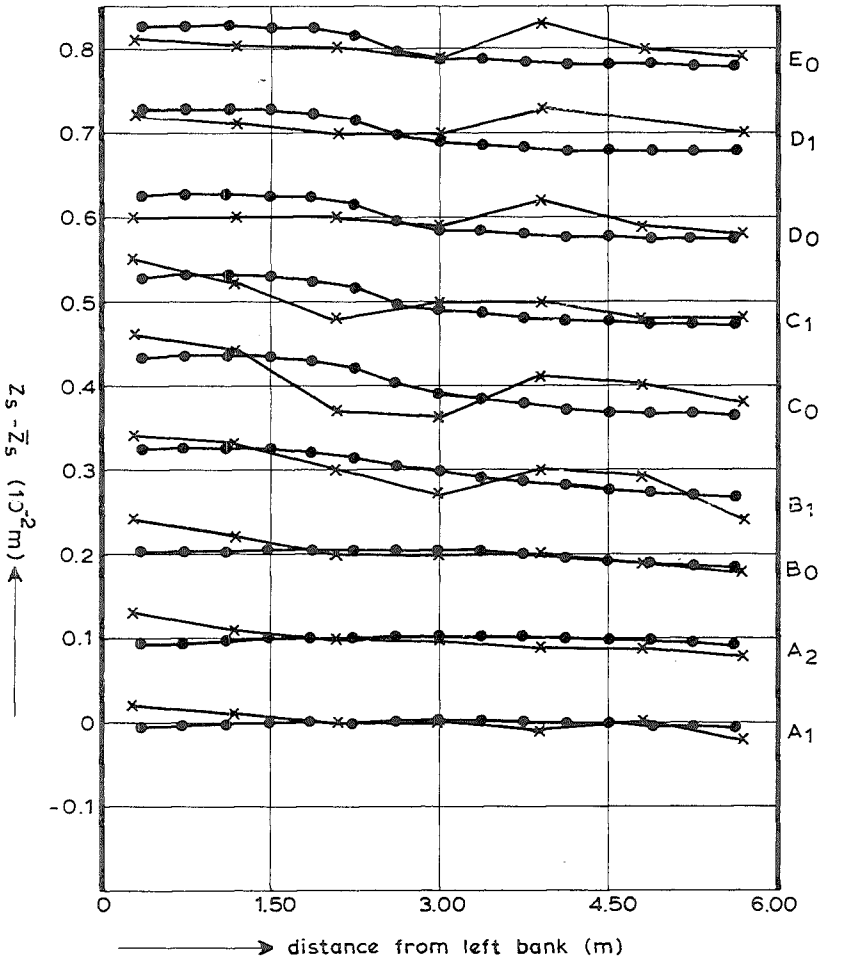

Ⓑ Q = 0.232 m^3/s

measured

computed

Ⓐ The water surface elevation scale is given for section A_1; in the subsequent sections $Z_s - \bar{Z}_s$ has been raised by 0.4×10^{-2} m every time

Ⓑ The water surface elevation scale is given for section A_1; in the subsequent sections $Z_s - \bar{Z}_s$ has been raised by 0.1×10^{-2} m every time

DELFT HYDRAULICS LABORATORY/DELFT UNIVERSITY OF TECHNOLOGY
R657/M1415
FIG. 13
T 9 - 1.2

TRANSVERSE CONFIGURATION OF THE ENERGY HEAD

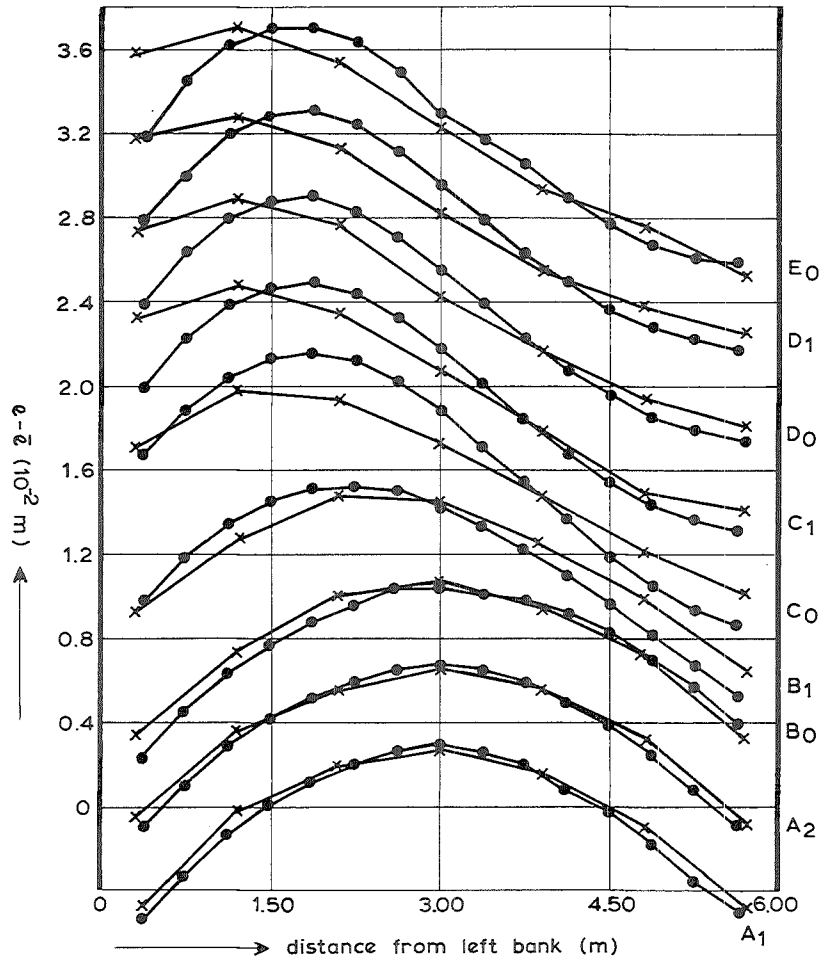

Ⓐ Q = 0.463 m³/s

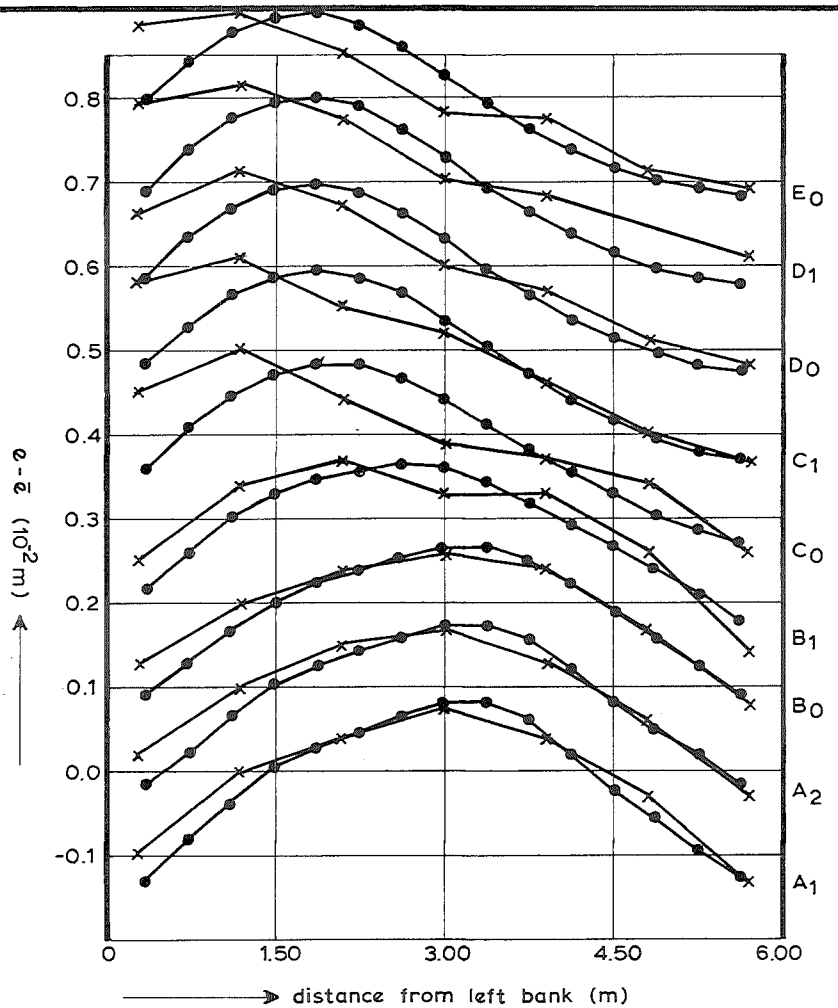

Ⓑ Q = 0.232 m³/s

measured
computed

Ⓐ The energy head scale is given for section A_1; in the subsequent sections $e-\bar{e}$ has been raised by 0.4×10^{-2} m every time

Ⓑ The energy head scale is given for section A_1; in the subsequent sections $e-\bar{e}$ has been raised by 0.1×10^{-2} m every time

DELFT HYDRAULICS LABORATORY/DELFT UNIVERSITY OF TECHNOLOGY | R657/M1415 | FIG. 14

appendices

Appendix A

INSTRUMENTATION

LIST OF FIGURES

INSTRUMENTATION

1 Water surface elevation

The water surface elevation was measured with static tubes connected to a measuring pit by plastic hoses of about 15 m length (see Figure 1). Three cross-sections could be reached from one pit, which implies that three pits were needed to cover all nine cross-sections. In each pit 7 measuring glasses were mounted, sothat for each cross-section the water surface elevations in all 7 measuring points could be recorded simultaneously. The water levels in the glasses were measured by point gauges. Using a vernier fine setting an accuracy in the readings of about 10^{-4} m could be obtained. The point gauge readings were related to the same horizontal datum as was used for the measurements of the bed elevation (see Figures 2a and b).

As a consequence of the rather long connections between the static tubes and the measuring glasses, a considerable time (several hours) elapsed between the installation of the tubes and the setting of the point gauges in order to have oscillations of the water in the measuring system damped out.

2 Flow velocity

The magnitude and the direction of the flow velocity were measured simultaneously by a combined current-velocity/direction meter, consisting of a miniature propeller and a vane (see Figure A1). The propeller measuring the magnitude of the velocity vector had a diameter of 0.011 m, while the vane indicating the direction of the velocity vector was 0.020 m high and 0.050 m long. By means of a servo-system the frame in which the propeller and the vane are mounted was turned in the flow direction, so that the propeller measures the total velocity v_{tot}. For more technical information see D.H.L. 1975.

The angular speed of the propeller varied linearly with the current velocity. A calibration curve (Figure A2) of the propeller gave the coefficients c_1 and c_2, necessary to convert the observed frequency (number of recorded pulses N divided by the time T) to the velocity:

$$v_{tot} = c_1 N/T + c_2 \qquad (A.1)$$

The calibration was executed in water with a certain temperature, which implied that the coefficients c_1 and c_2 should be corrected for the actual temperature of the water in the channel. In this respect it can be remarked that only c_2 varied with the water temperature to a considerable extent, depending on the individual propeller (Brolsma, 1973). A rough indication of this dependency, used for the present measurements, is given by:

$$c_{2actual} = c_{2calibration} + 0.0234\ (\eta_m - \eta_0) \quad (m/s), \tag{A.2}$$

in which:

η_m = the dynamic viscosity (in cp) of the water at the measuring temperature

η_0 = the dynamic viscosity (in cp) of the water during the calibration

3 Flow direction

The vane turns in the flow direction and commands the frame also to turn in the flow direction by means of two position sensors and a servo-system. The position of the frame is measured by means of a potentiometer. Since the flow is turbulent, the direction of the vane varies in time. The average reading s of the potentiometer over a set period is determined by using an electronic integrator. It is converted to the angle ϕ by:

$$\phi = c_3(s - s_o) \quad (radius)\ , \tag{A.3}$$

in which $c_3 = 0.00031$ is a coefficient of proportionality, and s_o is the reading of the potentiometer for a certain reference angle of the direction meter. This reference reading is obtained by calibrating the direction meter dynamically in a towing tank.

The instrument used during the present series of measurements (see Figure A1) was different from that used during the first series: a different system for the vertical positioning of the current-velocity/direction meter improved the accuracy of the flow direction measurements considerably. This accuracy is discussed in Appendix B.

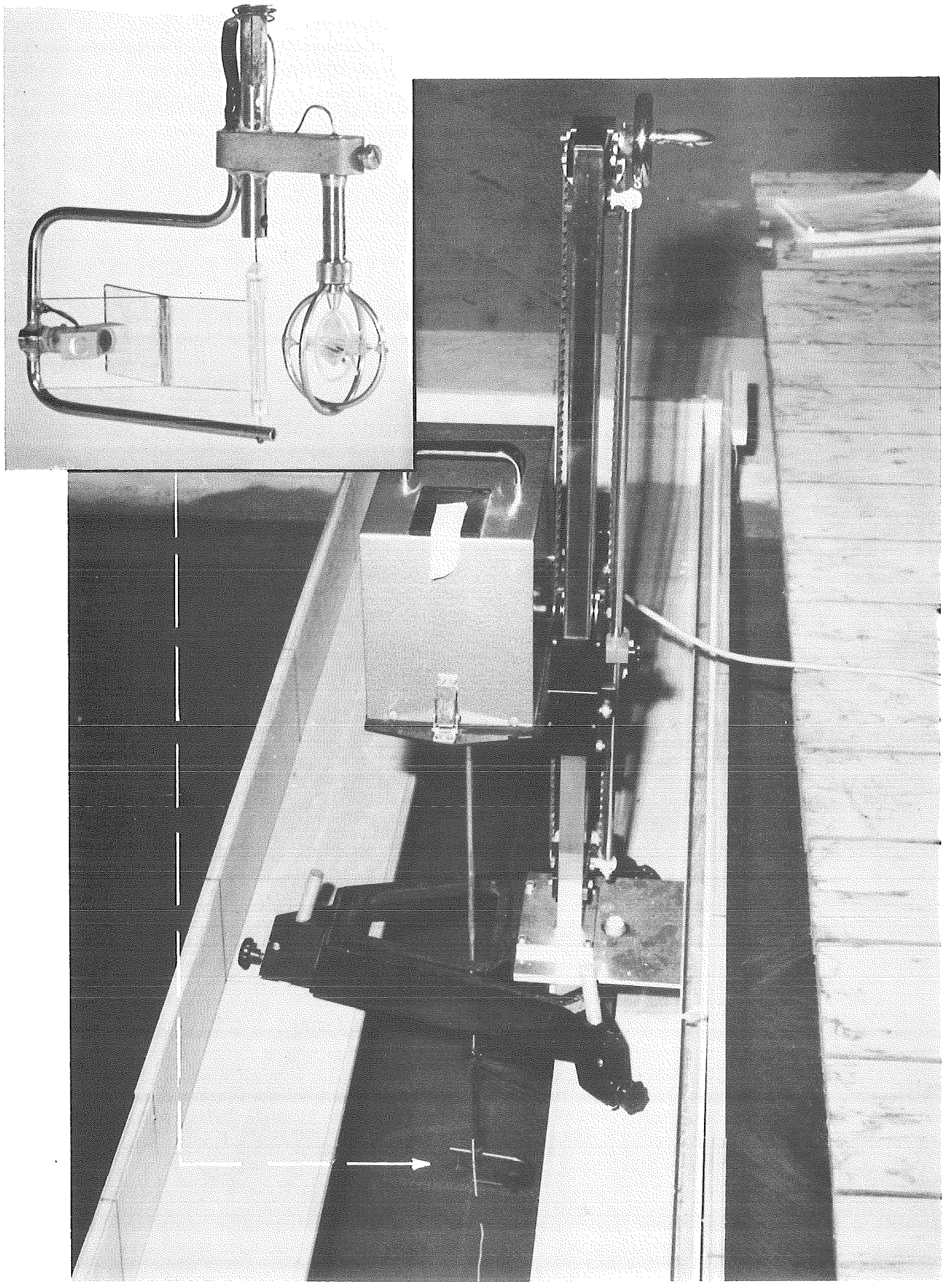

Figure A1 Combined current-velocity/direction meter

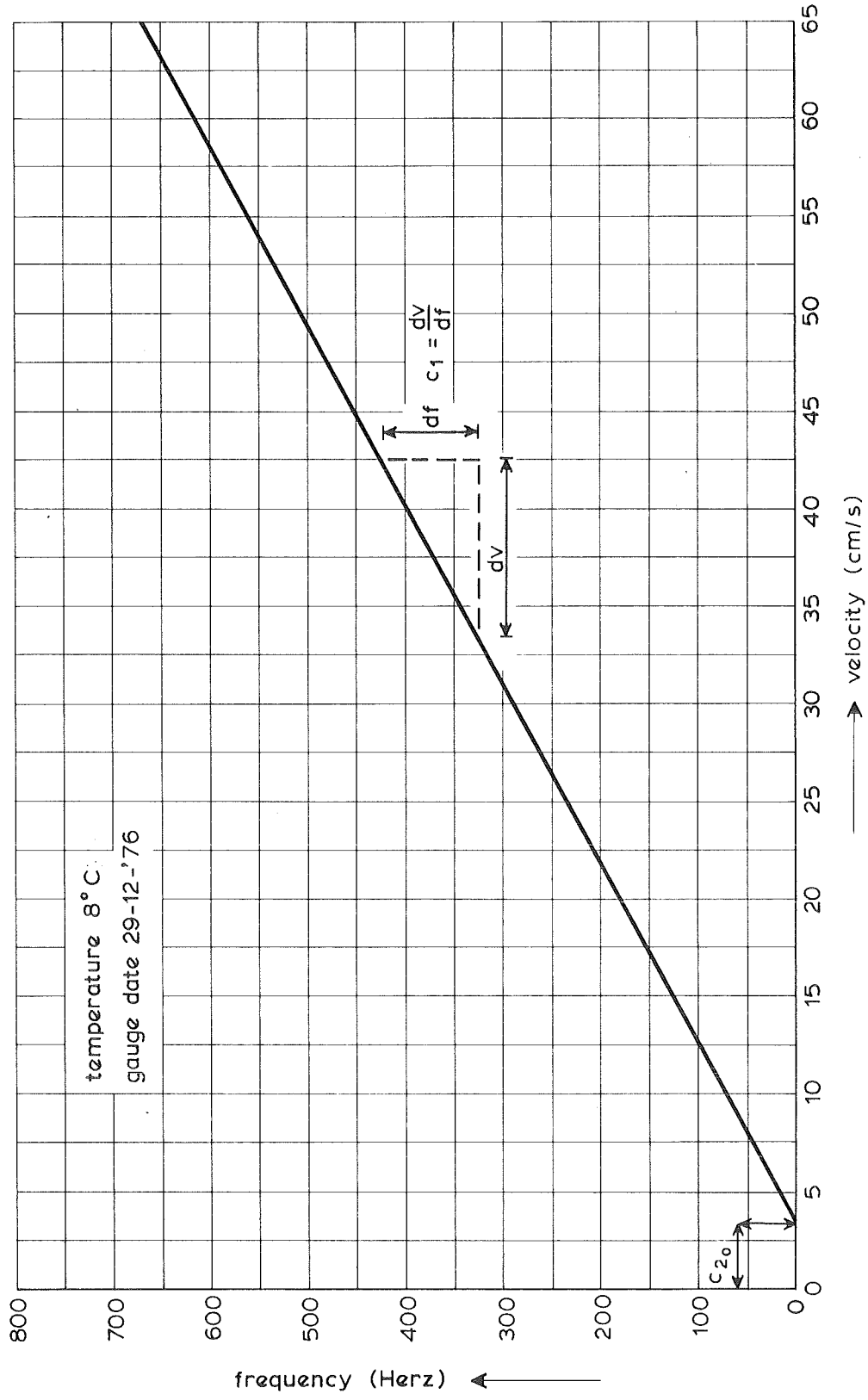

CALIBRATION CURVE VELOCITY METER

DELFT HYDRAULICS LABORATORY/DELFT UNIVERSITY OF TECHNOLOGY | R657/M1415 | FIG. A 2

Appendix B

MEASURING PROCEDURE

LIST OF TABLES

MEASURING PROCEDURE

1 Accuracy

1.1 Velocity measurements

As was shown for the plane bed experiments, observations of 30 s duration are sufficient for the flow velocity measurements. For the flow direction measurements, however, observations with a duration of 60 s are needed. As the flow velocity and the flow direction were being measured simultaneously, an observation period of 60 s was also used for the velocity measurements.

To obtain information about the accuracy of a measuring procedure with an observation period of 60 s, some additional velocity measurements were taken. In vertical D_0 4 30 subsequent observations were recorded at different heights above the bed. The coefficient of variation (see Table B1) gives an indication of the accuracy in relation to the vertical position above the bed. Observations close to the bed appear to be the least accurate.

1.2 Flow direction measurements

Like the current-velocity/direction meter used for the plane bed measurements, the present instrument was developed for measurements in larger-scale tidal models, where an accuracy of some degrees is sufficient. The accuracy of the flow direction measurements with this instrument has been tested extensively (Koch, 1977). These tests showed that the accuracy and calibration of the instrument depended on the flow conditions in which the observations are made. Therefore the direction meter was tested in the curved channel itself, in order to draw up a measuring procedure for the direction measurements. In different grid points a series of 30 flow direction observations was recorded, with the position of the instrument remaining unaltered during the series. The results, given in Table B2, show that the accuracy for an observation period of 60 s corresponds with a standard deviation of about 10 mV, or 0.2°. A substantial increase of this accuracy would require much longer observation periods.

Other sources of errors in the direction measurements are:
a. The procedure of calibration of the instrument;

b. the positioning of the cross-section; and
c. the vertical positioning of the instrument.

a Errors due to the calibration procedure

The direction meter was calibrated dynamically in a towing tank (Koch, 1977). Unfortunately the calibration did not yield a single value corresponding with a certain reference, but the calibration value was dependent on the flow conditions, such as flow velocity, depth of flow, distance from the bed. Consequently, an error of about 0.2^{o} has to be taken into account, and this error was even increased by another 0.5^{o} for measurements close to the water surface.

b Errors due to the positioning of the cross-section

The error in the reference angle introduced when placing the instrument in the cross-section depends on the accuracy of positioning the cross-section itself and on the accuracy of placing the instrument perpendicular to it. The standard deviations of the errors due to these two sources are estimated at 0.05^{o}.

c Errors due to the vertical positioning

The direction meter used during the plane bed experiments gave rise to a most serious error of 1^{o} to 5^{o} due to a backlash in the sliding transmission between the recording system and the vertical shaft in which the vane was mounted. When the vertical position of the present direction meter was changed, both the recording system and the vane moved vertically, so that no sliding transmission between these parts was needed. Still a systematic error could be introduced if the vertical beam along which the whole instrument was moved shows some torsion. Such an error can be measured and taken into account (Koch, 1977). The errors of this type turned out to be so small that they could be neglected here.

So the two most important errors in the direction measurements are: an error of 0.2^{o} due to the short duration of the measurement in turbulent flow, and another error of 0.2^{o} due to the calibration of the instrument.

Finally, the correlation between the errors in the velocity and the direction of the flow was investigated. The results are shown in Table B3, from which it was concluded that there is hardly any correlation between these two errors.

2 Measuring procedure

2.1 Positioning of the flow meter and the static tubes

The position of the cross-sections and verticals was fixed using the same movable support bridge (Figure A1) as during the flat bed experiments (de Vriend and Koch, 1977).

The fixed bed was taken as a reference for the position of the grid points in a vertical. The distance below the lowest point of the measuring device and the axis of the propeller was about 0.025 m, and by placing the lowest point of the instrument just above the bed, the velocity and deviation angles at 0.025 m above the bed could be measured. The highest measuring point was situated as close as possible to the free water surface, which meant that the axis of the propeller was about 0.02 m below the surface. The distance between the lowest and highest points was divided into at most 9 equal intervals, yielding at most 10 grid points in a vertical. If the depth of flow was too small to have 9 intervals of more than 0.01 m, the number of measuring points was reduced so, that the distance between the highest and the lowest points was divided into a number of intervals of about 0.01 m length. The accuracy of the vertical positioning was about 0.0005 m, which was thought to be sufficient.

The static tubes were mounted on a transportable bar across the channel, as was described for the plane bed experiments.

2.2 Velocity measurements

During the velocity measurements the magnitude and the direction of the velocity vector were measured twice during 60 s. The measurements started in the lower grid point and successively moved up to the surface point, where two subsequent observations were taken. Then successively lower points were revisited until the point near the bed was reached again. The apparatus was then removed from the water, the propeller was cleaned and the measurements restarted in the next vertical. All measurements, both for the similarity of the velocity distributions and for the depth-averaged velocity field, were executed in the 13 verticals of the cross-sections A_1, ..., E_0.

2.3 Surface elevation measurements

During both series of the velocity measurements (T7 and T8), the water surface elevation was measured every few hours in the verticals 1, 3, 5, 7, 9, 11 and 13 of the cross-section in which velocity measurements were taken at that moment. If more than one value per vertical was measured, the observed elevations were averaged in order to find "the" elevation in the relevant vertical.

level above bed	pulses $\bar{n}$ [1)]	stand. dev. σ_n	coeff. of variation 100 $\sigma_n/\bar{n}$
m	-	-	%
0.025	23361	308.9	1.32
0.102	28043	278.9	0.99
0.179	29294	178.6	0.61
0.256	29159	102.9	0.35
0.333	27567	130.4	0.47

1) Average number of pulses of 30 velocity observations of 60 s duration

Table B1 Accuracy of velocity measurements

duration of observation (s)	standard deviation of 30 observations (m V)							1 m V = 0.01775°
	vertical A_2 7				vertical D_0 4			
	z = 0.025 m	z = 0.046 m [1]	z = 0.138 m	z = 0.239 m	z = 0.025 m	z = 0.177 m	z = 0.297 m [1]	z = 0.333 m
5	53.8	21.5	35.6	30.7	57	18.5	28.0	25.7
10	37.0	7.2	21.8	20.4	34	12.6	20.9	19.0
15	33.6	13.3	17.3	16.6	33	10.7	18.5	16.1
20	29.1	11.6	16.6	15.9	24	8.9	13.4	12.3
30	24.1	7.7	13.7	15.1	16	8.4	10.2	11.7
45	21.8	3.9	13.7	11.6	20	9.0	8.4	10.3
60	16.2	3.8	12.2	9.9	12	8.3	3.6	10.4
75	13.9	5.2	12.0	8.8	12	8.1	4.2	9.1
90	13.2	4.8	11.7	8.3	12	8.1	4.0	8.3
105	11.8	5.2	12.0	8.0	11	7.7	2.2	8.0
120	11.5	4.4	11.9	8.4	10	7.8	2.4	7.6
150	10.7	3.9	11.8	8.1	10	7.0	1.8	7.4
180	9.0	3.4	11.7	7.8	10	7.0	2.3	7.2
210	7.9	1.0	11.1	8.4	9	7.0	2.4	6.2
240	7.9	1.2	11.4	7.9	8	6.5	1.8	5.8
270	7.0	1.2	11.1	7.7	8	6.2	1.4	5.2
velocity (m/s)	0.39	0.49	0.48	0.48	0.40	0.48	0.48	0.46

[1] 5 instead of 30 observations

Table B2 Accuracy of direction measurements

level above bed	pulses $\bar{n}$ [1]	stand. dev. T_n	deviation angle $\bar{\phi}$ [1]	stand. dev. T_ϕ	covariance cov(n,ϕ)	coeff. of correlation
m			degrees	degrees		
0.025	23702	370	-1.96	0.21	17.1	0.22
0.181	29672	198	0.50	0.05	3.29	0.33
0.338	28120	118	1.71	0.06	-2.41	-0.34

[1] Average of 30 observations of 60 s duration (T6-1)

Table B3 Correlation of the errors in the velocity and the direction measurements

Appendix C

ELABORATION OF MEASURED DATA

ELABORATION OF MEASURED DATA

The main outlines of the procedure used to translate the measured data into main and helical velocity components are the same as in the procedure used to elaborate the rectangular channel data (de Vriend and Koch, 1977). Referring to the relevant report, in which this procedure is described extensively, the unaltered steps will just be indicated here.

1 Magnitude and direction of the velocity vector

The magnitude of the measured velocity is computed from:

$$v_{tot} = c_1 \, N/T + c_2 \text{ with } c_2 = c_{2_0} + c_4(\eta_m - \eta_0) \qquad (C.1)$$

where:

N	=	number of pulses counted by the velocity meter during the observation period
T	=	duration of the observation period
c_1, c_{2_0} c_4	=	constants determined by calibration
η_m	=	dynamic viscosity of water at the measuring temperature
η_0	=	dynamic viscosity of water at the calibration temperature

The direction of the velocity vector with respect to the channel axis follows from:

$$\phi = c_3 \, (\phi' - \phi'_o) \, , \qquad (C.2)$$

where:

c_3	=	constant (here $c_3 = 1$)
ϕ'	=	reading of the flow direction meter
ϕ'_o	=	reference reading of the flow direction meter when the vane is parallel to the channel axis (see Koch, 1977).

2 Tangential and radial velocity components

The velocity components v_t and v_r, parallel and perpendicular to the channel axis respectively, are calculated from:

$$v_t = v_{tot} \cos\phi \quad \text{and} \quad v_r = v_{tot} \sin\phi \tag{C.3}$$

3 Magnitude and direction of the depth-averaged velocity vector

At this point the present procedure substantially deviated from the former one. To avoid the trapezoidal integration rule, which is a severe source of errors due to the relatively large distance from the lowest measuring point to the bed (de Vriend, 1978), the following assumptions were made as to the vertical distributions of the main and the helical velocity components:

$$v_{main} = \tilde{v}_{main} f_{main} (\tfrac{z}{h}) \tag{C.4}$$

where:

$$f_{main} = 1 + \frac{\sqrt{g}}{\kappa C} + \frac{\sqrt{g}}{\kappa C} \ln(\tfrac{z}{h}) \tag{C.5}$$

$$v_{hel} = \tilde{v}_{hel} f_{sec} (\tfrac{z}{h}) \tag{C.6}$$

where:

$$f_{sec} = \frac{1}{\kappa^2} \{2F_1 (\tfrac{z}{h}) + \frac{\sqrt{g}}{\kappa C} F_2 (\tfrac{z}{h}) - 2(1 - \frac{\sqrt{g}}{\kappa C}) f_{main} (\tfrac{z}{h})\} \tag{C.7}$$

$$F_1 (\tfrac{z}{h}) = \int_{z_o^*/h}^{z/h} \frac{\ln (\frac{z}{h})}{\frac{z}{h} - 1} d(\tfrac{z}{h}) \quad \text{with} \quad \frac{z_o^*}{h} = \exp(-1 - \frac{\kappa C}{\sqrt{g}})$$

$$F_2 (\tfrac{z}{h}) = \int_{z_o^*/h}^{z/h} \frac{\ln^2 (\frac{z}{h})}{\frac{z}{h} - 1} d(\tfrac{z}{h})$$

Theoretically, $\tilde{v}_{main} = \bar{v}_{main}$ and $\tilde{v}_{hel} = \bar{v}_{main} \frac{h}{R_s} \approx \bar{v}_{main} \frac{h}{R}$ (de Vriend, 1976 and 1977).

The definition of the total mean velocity reads:

$$\bar{v}_{tot} = (\bar{v}_t^2 + \bar{v}_r^2)^{\frac{1}{2}} \tag{C.8}$$

$$= \left[\{\frac{1}{h} \int_0^h v_{tot} \cos\phi \, dz\}^2 + \{\frac{1}{h} \int_0^h v_{tot} \sin\phi \, dz\}^2 \right]^{\frac{1}{2}}$$

$$= \left[\{\frac{1}{h} \int_0^h v_{tot} \cos(\phi-\alpha) \cos\alpha \, dz - \frac{1}{h} \int_0^h v_{tot} \sin(\phi-\alpha) \sin\alpha \, dz\}^2 + \right.$$

$$\left. + \{\frac{1}{h} \int_0^h v_{tot} \sin(\phi-\alpha) \cos\alpha \, dz + \frac{1}{h} \int_0^h v_{tot} \cos(\phi-\alpha) \sin\alpha \, dz\}^2 \right]^{\frac{1}{2}}$$

If α is the direction of the streamlines of the depth-averaged flow field with respect to the channel axis (positive outwards), v_{main} and v_{hel} are defined by:

$$v_{main} = v_{tot} \cos(\phi-\alpha) \quad \text{and} \quad v_{hel} = v_{tot} \sin(\phi-\alpha) \tag{C.9}$$

Hence $\bar{v}_{tot}$ can be written as

$$\bar{v}_{tot} = \left[\{\frac{1}{h} \int_0^h v_{main} \, dz\}^2 \quad \{\frac{1}{h} \int_0^h v_{hel} \, dz\}^2 \right]^{1/2} \tag{C.10}$$

As the streamline direction α is defined by

$$\tan\alpha = \frac{1}{h} \int_0^h v_{tot} \sin\phi \, dz \, / (\frac{1}{h} \int_0^h v_{tot} \cos\phi \, dz) \tag{C.11}$$

the mean helical velocity vanishes:

$$\frac{1}{h} \int_0^h v_{hel} \, dz = \frac{1}{h} \int_0^h v_{tot} \sin(\phi-\alpha) \, dz \, ,$$

$$= \frac{\cos\alpha}{h} \int_0^h v_{tot} \sin\phi \, dz - \frac{\sin\alpha}{h} \int_0^h v_{tot} \cos\phi \, dz = 0 \, . \tag{C.12}$$

Consequently:

$$\bar{v}_{tot} = \frac{1}{h} \int_0^h v_{main} \, dz = \bar{v}_{main} \tag{C.13}$$

so theoretically (C.4) is equivalent to

$$v_{main} = \bar{v}_{tot} \, f_{main} \, (\frac{z}{h}) \tag{C.14}$$

Adopting a least squares method to fit $f_{main} \, (\frac{z}{h})$ to the measured data, $\tilde{v}_{main}$

is determined in such a way, that the mean square of the differences between V_{main} (calculated from the measured data) and v_{main} as calculated by (C4), is minimized in a vertical. This leads to:

$$\tilde{v}_{main} = \frac{\sum_{i=1}^{np} V_{main_i} f_{main} (\frac{z_i}{h})}{\sum_{i=1}^{np} f^2_{main} (\frac{z_i}{h})} \qquad (C.15)$$

To calculate V_{main} from the measured data, however, the streamline angle α needs to be known. This quantity is determined in a similar way.
Equations (C.4), (C.6) and (C.9) lead to:

$$\tan(\phi-\alpha) = \frac{\tilde{v}_{hel}}{\tilde{v}_{main}} f_\phi (\frac{z}{h}) \quad \text{with} \quad f_\phi (\frac{z}{h}) = \frac{f_{sec} (\frac{z}{h})}{f_{main} (\frac{z}{h})} \qquad (C.16)$$

For small values of α, this can be elaborated to

$$\tan\phi \approx \frac{\tilde{v}_{hel}}{\tilde{v}_{main}} f_\phi (\frac{z}{h}) + \tan\alpha \ . \qquad (C.17)$$

So if the tangent of the measured flow angle is expressed by

$$\tan\Phi = a_1 f_\phi (\frac{z}{h}) + a_2 \ , \qquad (C.18)$$

the theoretical values of a_1 and a_2 are $\frac{h}{R}$ and $\tan\alpha$ respectively. When applying the least squares method to determine a_1 and a_2 from the measured data in a vertical, two linear equations in these quantities are found:

$$A\ a_1 + B\ a_2 = C \quad \text{and} \quad B\ a_1 + np\ a_2 = D \ , \qquad (C.19)$$

in which:

$$A = \sum_{i=1}^{np} f^2_\phi (\frac{z_i}{h})$$

$$B = \sum_{i=1}^{np} f_\phi (\frac{z_i}{h})$$

$$C = \sum_{i=1}^{np} f_\phi (\frac{z_i}{h}) \tan\Phi_i$$

$$D = \sum_{i=1}^{np} \tan\Phi_i$$

The solution of (C19) for $B^2 \neq np\ A$ reads:

$$a_1 = \frac{np\ C - BD}{np\ A - B^2} \quad \text{and} \quad a_2 = \frac{AD - BC}{np\ A - B^2} \quad . \tag{C.20}$$

Thus least squares approximations of $\bar{v}_{main} = \bar{v}_{tot}$ ($\approx \tilde{v}_{main}$; see (C15)), α ($\approx \text{atan}\ a_2$) and $\tilde{v}_{hel}$ ($\approx \frac{h\ \tilde{v}_{main}}{R}$) are obtained.

4 Main and helical velocity components

The local main and helical velocity components are calculated from:

$$v_{main} = v_{tot} \cos(\phi-\alpha) \quad \text{and} \quad v_{hel} = v_{tot} \sin(\phi-\alpha) \tag{C.21}$$

It should be noted that the former component has already been determined in the foregoing step when computing $\tilde{v}_{main}$.

5 Normalization

The main and helical velocity components are normalized by:

$$v'_{main} = \frac{v_{main}}{\bar{v}_{tot}} \quad \text{and} \quad v'_{hel} = \frac{v_{hel}}{\tilde{v}_{hel}} \quad . \tag{C.22}$$

The latter definition differs from the one in the rectangular channel procedure in that $\tilde{v}_{hel}$ is used instead of its theoretical value $\bar{v}_{tot}\ \frac{h}{R}$.